มหาวิทยาลัยขอนแก่น
KHON KAEN UNIVERSITY

รายงานวิจัยฉบับสมบูรณ์

โครงการ การศึกษาเชิงอิเล็กทรอนิกส์ เชิงแสง และเชิงการดูดซับไฮโดรเจนของวัสดุพื้นผิวสูง

Title Computational Studies of electronic, optical and hydrogen adsorption properties of high-surface area materials

โดย ผศ. ดร. พรจักร ศรีพัชราวุธ และ คณะ

มิถุนายน 2557

สัญญาเลขที่ MRG5580055

รายงานวิจัยฉบับสมบูรณ์

โครงการ การศึกษาเชิงอิเล็กทรอนิกส์ เชิงแสง และเชิงการดูดซับไฮโดรเจนของวัสดุพื้นผิวสูง

Title Computational Studies of electronic, optical and hydrogen adsorption properties of high-surface area materials

ผู้วิจัย **สังกัด**

1. **ผศ. ดร. พรจักร ศรีพัชราวุธ** **ภาควิชาฟิสิกส์ คณะวิทยาศาสตร์ มหาวิทยาลัยขอนแก่น**
2. **รศ. ดร. วิทยา อมรกิจบำรุง** **ภาควิชาฟิสิกส์ คณะวิทยาศาสตร์ มหาวิทยาลัยขอนแก่น**

สนับสนุนโดยสำนักงานคณะกรรมการการอุดมศึกษา สำนักงานกองทุนสนับสนุนการวิจัย และ มหาวิทยาลัยขอนแก่น

บทคัดย่อ

รหัสโครงการ: MRG5580055

ชื่อโครงการ: การศึกษาเชิงอิเล็กทรอนิกส์ เชิงแสง และเชิงการดูดซับไฮโดรเจนของวัสดุพื้นผิวสูง

ชื่อนักวิจัย: ผศ. ดร. พรจักร ศรีพัชราวุธ

E-mail Address: spornj@kku.ac.th

ระยะเวลาโครงการ: กรกฎาคม 2555 - กรกฎาคม 2557

โครงการวิจัยนี้เกี่ยวข้องกับการศึกษาเชิงคำนวณคุณสมบัติเชิงอิเล็กทรอนิกส์ เชิงแสง และเชิงการดูดซับไฮโดรเจนของวัสดุพื้นผิวสูงโดยอาศัยทฤษฎีฟังก์ชันนัลความหนาแน่น สำหรับระบบ Covalent triazine based framework-1 (CTF-1) ผู้วิจัยทำการปรับแต่งโครงสร้างดังกล่าวด้วยการแทนที่อะตอม N ทุกอะตอมด้วย P, As และ Sb โดยพบว่าช่องว่างแถบพลังงานมีค่าอยู่ในช่วง 0 ถึง 2.02 eV นอกจากนี้ ผู้วิจัยได้ทำการเปลี่ยนแปลงความเข้มข้นของ P และ As ในโครงสร้าง CTF-1 และพบว่าช่องว่างแถบพลังงานลดลงอย่างไม่เป็นเชิงเส้น นอกจากนี้ผู้วิจัยได้เสนอวิธีเพิ่มพลังงานดูดซับไฮโดนเจนในวัสดุ Covalent Organic Framework-366 (COF-366) และ Zeolitic Imidazolate Framework-23 (ZIF-23) โดยในรายงานวิจัยฉบับนี้ ผู้วิจัยได้ทำการปรับปรุงพลังงานดูดซับไฮโดรเจนโดย (1) การเติมแต่งโลหะ Li ลงบนพื้นผิวของวัสดุ COF-366 และ การขยายส่วนของโลหะไนไตรด์คลัสเตอร์ในวัสดุ ZIF-23 สำหรับวัสดุ COF-366 ที่ถูกเติมแต่งด้วย Li ผู้วิจัยพบว่าพลังงานยึดเหนี่ยวไฮโดรเจนมีค่าอยู่ในช่วง 0.03 ถึง 0.22 eV/H_2 นอกจากนี้ ผู้วิจัยได้ทำการคำนวณความสามารถในการกักเก็บไฮโดรเจนของโครงสร้างดังกล่าว โดยพบว่าปริมาณดังกล่าวมีค่าเท่ากับ 2.06 1.58 และ 1.05 เปอร์เซนต์โดยน้ำหนักที่ความดันปกติและอุณหภูมิ 77 150 และ 298 เคลวิน ตามลำดับ สำหรับโครงสร้าง ZIF-23 ผลการคำนวณแสดงให้เห็นว่า โมเลกุลไฮโดรเจนไม่เกาะบนสาย 4-Azabenzimidazolate สำหรับแหล่งดูดซับใกล้กับโลหะไนไตรด์คลัสเตอร์ ผู้วิจัยพบว่าพลังดูดซับที่แหล่งดูดซับดังกล่าวแปรผันตรงกับรัศมีอะตอมของโลหะในไนไตรด์คลัสเตอร์

คำสำคัญ: ช่องว่างแถบพลังงาน พลังงานดูดซับไฮโดรเจน Covalent Triazine based Framework-1 Covalent Organic Framework-366 Zeolitic Imidazolate Framework-23

Abstract

Project Code: MRG5580055

Project Title: Computational Studies of electronic, optical and hydrogen adsorption properties of high-surface area materials

Investigator: Asst. Prof. Pornjuk Srepusharawoot

E-mail Address: spornj@kku.ac.th

Project Period: July 2012 – July 2014

This Project deals with the computational studies of electronic, optical and hydrogen adsorption properties of three types of high-surface area materials by means of the density functional theory. For Covalent Triazine based Framework-1 (CTF-1), we modified the CTF-1 structure by replacing all N atoms with P, As and Sb. Our results shown that energy gaps are ranged from 0.0 to 2.02 eV. Moreover, we also varied the concentrations of P and As in the CTF-1 structure and found that non-linear drop of energy gap is observed. In this report, we also proposed two methods for enhancing the hydrogen physisorption energy by (1) functionalizing hydrogen attracting metal, Li into the Covalent Organic Framework-366 (COF-366) and (2) opening metal nitride cluster of Zeolitic Imidazolate Framework-23 (ZIF-23). According to the results of Li decorated COF-366, we found that the hydrogen adsorption energies are ranged from 0.03 to 0.22 eV/H_2. In addition, the hydrogen capacity was also determined and found that it is 2.06 1.58 and 1.05 H_2 wt% for 77, 150 and 298 K and ambient pressure, respectively. For ZIF-23 structure, our results revealed that hydrogen molecule does not bind with 4-Azabenzimidazolate linker. For H_2 adsorption sites near metal nitride cluster, we found that the corresponding hydrogen adsorption energies are directly proportional to the atomic radius of metal in metal nitride cluster.

Keywords: Energy gap, Hydrogen adsorption energy, Covalent Triazine based Framework-1, Covalent Organic Framework-366, Zeolitic Imidazolate Framework-23

Contents

List of Figures

List of Figures (Cont.)

CHAPTER I

Introduction

It is a well known problem that the energy demand is increasing due to the enormous growing of industries in the world, whereas the current energy resources such as fossil fuel based resources start to be depleted. Moreover, by-products of most fossil fuels produce pollution affecting directly not only our health but also the environment leading to many severe effects e.g. global warming. Owing to these serious disadvantages, we need to find alternative energy resources which are abundant and environmental friendly.

One promising solution for this problem is to get energy from sunlight, so called "Solar Energy". Solar energy is one energy resource which is clean and abundant. We can get electricity from sunlight via the device, called Solar cells or photovoltaic devices. The principle of photovoltaic devices is that incident light is absorbed by materials such as crystalline and amorphous Si [1], GaAs [2], copper indium gallium diselenide (CIGS) [3]. Consequently, electrons are excited from their valence bands to their conduction bands. The excited electrons flow through the external load leading to current generation. In the photon spectra, the maximum photon intensity is in the range from 400 to 600 nm [4]. This wavelength region corresponds to an energy gap (E_g) of about 1.4–3.0 eV. Hence, a suitable E_g for any light absorber should also be in this range in order to maximize solar cell energy conversion efficiency. However, most of materials in nature do not have an E_g in this range. As a result, tuning the energy gap of materials into this desirable range is an essential technique which can be applied to photovoltaic devices and other optically related applications such as sensors [5] and light emitting diodes (LED) [6].

Another promising candidate for the future energy resources is energy from hydrogen. Hydrogen economy is presumed to be a promising candidate resource for replacing the currently used energy resources because hydrogen can be split from water which is very abundant in the world. In addition, non-toxic product, water, is formed from the reaction between protons and oxygen in the fuel cell. Various literatures [7-9] have shown that hydrogen possesses higher gravimetric energy density than the current energy resources such as methane and gasoline for about three times. In other words, one kilogram of hydrogen can produce the same amount of energy as 3 kg of gasoline as shown in Figure 1.1. However, one major serious

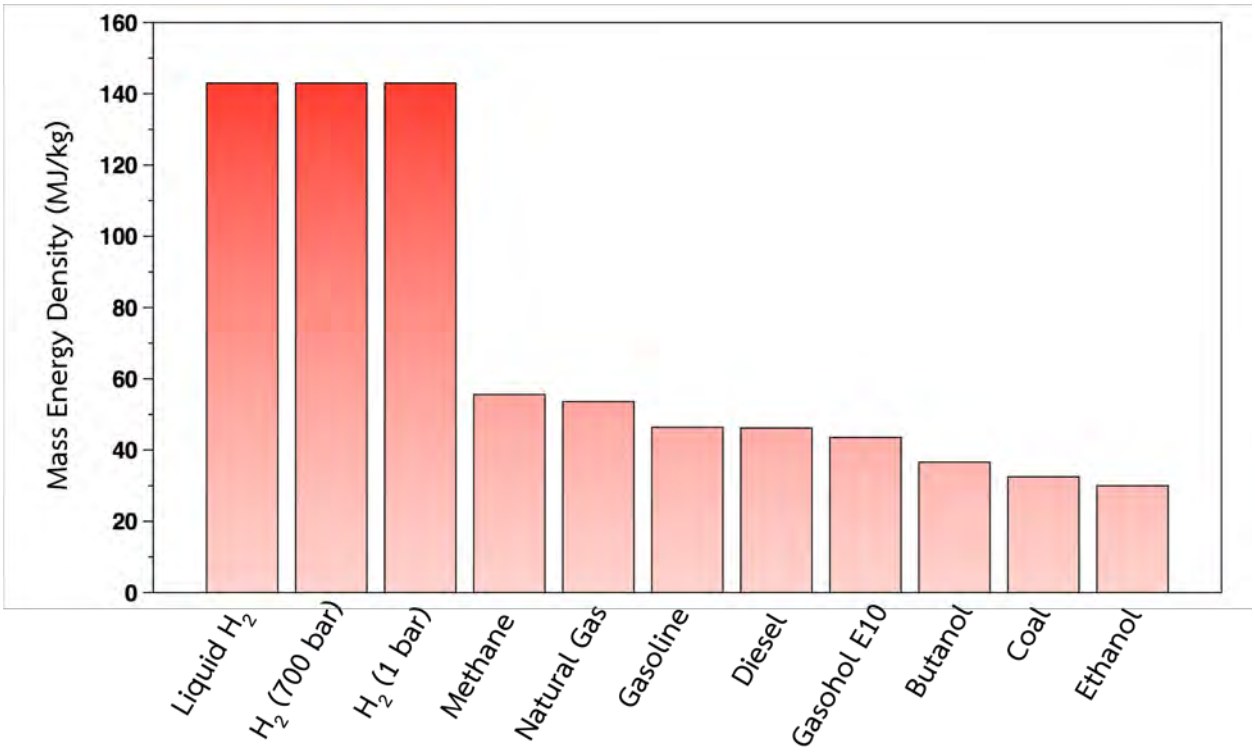

Figure 1.1 Mass energy density of various energy resources [10].

Obstacle to use hydrogen as an alternative energy resource is that the volumetric density of hydrogen gas is indeed low, namely 0.09 kg/m^3. Consequently, it requires a large amount of space for storing hydrogen and hence the so-called hydrogen storage problem arises. Currently, there are three different methods to trap hydrogen in the medium, namely gaseous, liquid and solid-state storages. For gaseous storage, it is very conventional method to trap gaseous hydrogen in the storage tank. However, the well-known problem for this method is that hydrogen gas has very low volumetric density, 0.09 kg/m^3 at 1 bar of pressure. As a result, the storage tank requires tremendous space to store hydrogen inside. From an industrial point of view, a hybrid car needs 4 kg of hydrogen for driving 400 km [7]. This amount of stored hydrogen corresponds to 45 m^3 of occupied volume at ambient condition. Hence, the storage tank must be extremely large and then it is unable to fit into the conventional storage tank. To improve the volumetric density, the most traditional way can be done by compressing hydrogen gas in the tank leading to gain hydrogen volumemetric density. However, the main problem when H_2 gas is pressurized in the tank is that the walls of the storage tank need to be well shielded for protecting the leakage of hydrogen gas. As a consequence, the tank is rather heavy in

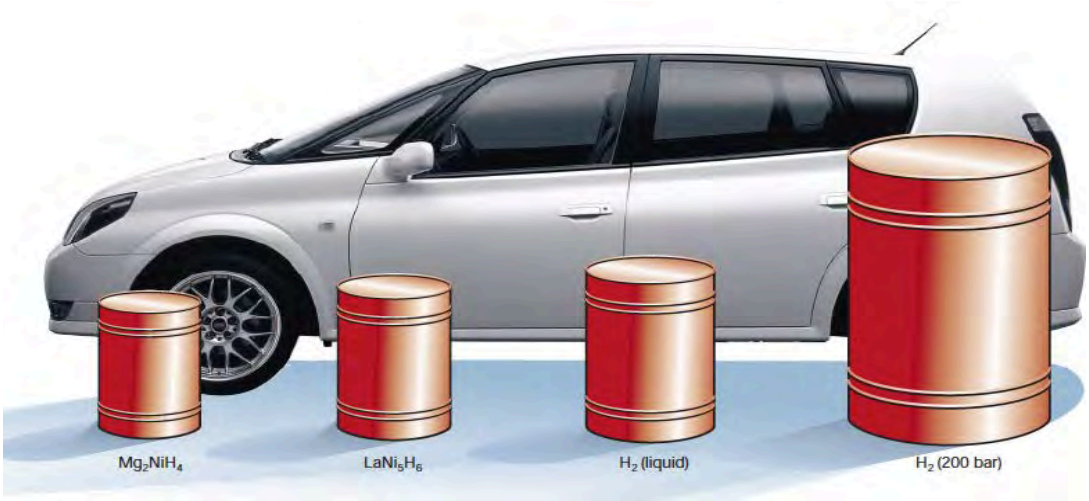

Figure 1.2 Various hydrogen storage media containing 4 kilogram of hydrogen [7].

comparison to the currently used hydrocarbon tanks resulting in inefficiency for mobile applications. In addition, safety issue, cost of pressurization, hydrogen embrittlement of hydrogen tank and sudden drop of pressure during use are other drawbacks of this storage method. Based on several drawbacks of gaseous storage as previously mentioned, liquid hydrogen or slush hydrogen has received attention because it possesses higher volumetric density than the gaseous state i.e 70.8 kg/m^3 for liquid hydrogen in comparison to 0.09 kg/m^3 for H_2 gas [11, 12]. Hence, the same amount of liquid hydrogen occupies smaller space than H_2 gas. However, the major disadvantage of this storage method is that liquid hydrogen exists only in a very low and narrow range of temperature, namely 21-32 K [11]. Moreover, an enormous amount of energy is needed for cooling down H_2 to reach the liquid state. In addition, the designed vessels need to be well insulated in order to prevent boil-off of H_2 coming from the hydrogen evaporation (about few percent per day at room temperature [11, 13]).

As clearly shown in Figure 1.2, sizes of the gaseous and liquid hydrogen tanks are explicitly seen to be bigger than those of storage media made from $LaNiH_6$ and Mg_2NiH_4. Consequently, keeping hydrogen in the suitable materials, so called “solid-state storage” is expected to be a promising approach of hydrogen storage materials. At ambient condition, molecular hydrogen or H_2 is a stable configuration. Once it approaches the host material surface, there is an induced dipole-induced dipole interaction or van der Waals interaction between non-dissociated hydrogen and host. This is so called the physisorption mechanism. Physisorption or

physical adsorption is a process in which the hydrogen molecule adheres to the host material's surface by weak dispersive interaction. Usually, this interaction strength is very weak, less than 10 kJ/mol. Hydrogen physisorption mechanism usually occurs in high-surface area materials such as carbon based materials [12, 14-17], metal organic frameworks (MOFs) [18-25], covalent organic frameworks (COFs) [26-30], zeolite [31,32], zeolitic imidazolate frameworks [33,34] and so on. The big advantage of this mechanism is straightforward H_2 adsorption/desorption at ambient condition leading to fast kinetic. On the downside, too weak interaction between trapped H_2 molecules and host framework results in requiring cryogenic temperature/high pressure to hold molecular hydrogen within the host material. In order to improve the hydrogen capacity in the physisorbed systems at room temperature, the hydrogen adsorption energy must be enhanced. Practically, the hydrogen storage media have to release hydrogen easily and trap hydrogen strongly. Hence the interaction between hydrogen molecules and host should not be too low or too high. The ideal hydrogen adsorption energy for hydrogen storage material should be about 40 kJ/mol for practical applications [35].

Based on theoretical and experimental studies, they have shown that high-surface area materials can be acted as gas storage media e.g. CO_2 [36, 37], CH_4 [38, 39], N_2 [40], Ar [41]. Moreover, they can also be applied in catalyst, sensors [42], and solar cell applications. For solar cell applications, especially in dye-sensitized solar cell (DSSC), electrons can be created by excitation process from valence band to conduction band of dye molecules and the excited electrons are injected to suitable materials such as ZnO or TiO_2 [43]. This leads to the fact that the more excited electrons from dye molecules, the more electricity generated from the DSSC. To obtain excited electrons as much as possible, the materials should contain numerous places for dye absorptions. Hence, the high-surface area materials shown an important role as promising materials used in the DSSC applications. Another important factor related to number of electrons transferred from the dye to the material is the energy levels between the material and dye. For good material in DSSC applications, usually, the lowest unoccupied energy level (LUMO) of dye molecules is slightly higher than the conduction band of materials. To maximize the DSSC efficiency, the band gap of materials has to be tunable. In the present work, the high-surface area materials, namely Covalent Triazine based Framework-1 (CTF-1 or CTF-N) [44-46] was chosen to investigate the electronic and optical properties. We also believed that it can be

applied as counter electrode in dye sensitized solar cell (detail of this part was discussed in Section 3.1 and Paper I). Another application of the high-surface area materials used as hydrogen storage medium is explained. Various types of high-surface area materials, for example, carbonaceous materials [12], metal organic frameworks (MOFs) [18-25], covalent organic frameworks (COFs) [26-30], zeolite [31], zeolitic imidazolate frameworks (ZIFs) [33, 34] and so on can be used as promising hydrogen storage materials. According to both theoretical and experimental studies of hydrogen storage in carbonaceous materials, activated carbon can store hydrogen up to 0.85 wt% at 100 bars of pressure and room temperature [47]. In addition, experimental results revealed that hydrogen capacities of single-walled carbon nanotubes can exceed 8 wt% at 80 K and 80-100 bar of pressure [48]. Recently, COFs and ZIFs have shown as the promising hydrogen storage because their crystal structures can be flexibly adjustment. At the same time, they also contains numerous number of hydrogen adsorption sites. To get high hydrogen uptake, an importance parameter related to this property is that mass of the high surface area material should be as low as possible. To satisfy this requirement, the materials must be synthesized from light elements such as B, C, O and H and we called these materials as the covalent organic frameworks or COFs. COFs can be used in various applications, for instance, hydrogen storage [27, 49,50], methane storage [51], CO_2 storage [52] and ammonia storage [53]. In addition, it can also be adopted in photoelectric and catalyst applications [54, 55]. For hydrogen storage application, COF-1 consisting of B_3O_3 ring covalently bonded with C_6H_4 rings. Its hydrogen capacity is 1.28 wt% at temperature of 77 K and ambient pressure [56]. Moreover, the hydrogen uptakes of other COFs at this condition are 3.58, 2.26, 3.50, 7.24 wt% for COF-5, COF-6, COF-8 and COF-102, respectively [52]. The increment of hydrogen uptake directly relates to the surface area of the host material. For CO_2 storage, COF-1 can adsorb CO_2 about 230 mg/g at room temperature and 55 bar of pressure [52]. This value is improved for other types of COFs. For example, COF-5 and COF-103 can bind CO_2 of 870 and 1190 mg/g, respectively [52]. For zeolitic imidazolate frameworks or ZIFs, they were successfully synthesized by Yaghi 's research group [57]. They can also be used as gas storage media [57, 58] such as H_2, Ar, N_2, CO_2 and CH_4. Based on neutron diffraction experiments [59], ZIF-8 can trap 28 hydrogen molecules at 30 K and ambient pressure corresponding to 4.2 H_2 wt%. By increasing the temperature to 77 K and 80 bar of pressure, the hydrogen capacity is slightly decreased to 3.1 wt% [60]. For another type of ZIFs, namely ZIF-23, there is no report in the

literature about the hydrogen adsorption mechanism in this material. This motivates us to focus on the ZIF-23 system.

However, both experimental and theoretical studies reveal that the interaction between hydrogen molecules and the high-surface area materials is indeed weak. To obtain higher hydrogen uptake in high-surface area materials, the interaction energy of these systems must be improved to the ideal hydrogen adsorption energy, about 40 kJ/mol [35]. Currently, there are several methods to improve the hydrogen adsorption energy. In this report, two promising approaches are discussed. The first method is to decorate hydrogen attracting metal e.g. Li [21, 61,62], Na [62], K[62], Ca [63,64], Ti [65,66] and so on into host materials 's surface resulting in charge transferred from metal to the host structure. Consequently, the metal is no longer to be neutral but it changes to metal ion. When hydrogen interacts to the metal ion, the interaction between hydrogen molecule and metal ion is electrostatic interaction leading to enhance the hydrogen adsorption energy. In Paper II, we improved the hydrogen adsorption energy by functionalizing Li on the Covalent Organic Framework-366 (COF-366). The hydrogen binding energy between Li and COF-366 structure at various adsorption sites were calculated. Moreover, the interaction energy between hydrogen molecule and Li was determined as well. Lastly, the hydrogen capacity of the Li functionalized COF-366 was evaluated. Detail description of this project was explained in Section 3.2 and Paper II in the appendix.

Another approach for enhancing the hydrogen adsorption energy in the high-surface area materials is to replace metal in the host with larger metal. The increasing in size of metal leads to a more-opening structure, allowing the H_2 molecules to approach closer and thus interact more strongly. Moreover, the opening in crystal structure results in a higher polarization and since the polarization is proportional to the van der Waals interaction which is the major interaction between hydrogen molecules and high-surface area materials. Hence the hydrogen adsorption energy is improved. Srepusharawoot *et al.* [67] showed that the hydrogen binding energies are increased for 15% when metal oxide cluster of MOF-5 is more-opening. In this report, we improved the hydrogen adsorption energy of ZIF-23 system based on the method previously discussed. For ZIF-23, it consists of metal nitride cluster and Imidazolate linker. We enhanced the hydrogen adsorption energy of three different structures, namely Be-ZIF-23, Zn-ZIF23 and Cd-ZIF23. Detail description of these structures can be found in Section 3.3 or Paper III in the appendix. Next, the hydrogen adsorption energy at all possible adsorption sites were investigated. Last, the hydrogen adsorption energy near the metal nitride cluster of M-ZIF23 (M= Be, Zn and Cd) were determined. Results of our investigation were discussed in Section 3.3.

CHAPTER II

Research Methodology

In this chapter, we classified the research methodology into three parts. In section 2.1, the many-electron system will be introduced. The density functional theory or DFT and Born-Oppenheimer Molecular Dynamics are explained in section 2.2 and 2.3, respectively.

2.1 Many-electron System

In reality, we always deal with the systems containing large number of atoms (about 10^{23} atoms) and hence we cannot escape from the many body problems. For many body problems, we focus only on solid containing of 10^{23} atoms. In solid, it contains many electrons and nuclei and the behavior of these particles must be obeyed the time-independent Schrödinger equation

$$\hat{H}\Psi(\vec{r},\vec{R}) = E\Psi(\vec{r},\vec{R}) \,, \tag{1}$$

where $\hat{H}$, E and Ψ are the Hamiltonian, energy eigenvalue and wave function of solid which is related to the probability to find an electron at position $\vec{r}$ and nucleus at position $\vec{R}$, respectively. In this case, we assume that solid consists of N_e electrons and N_{nuc} nuclei and the Hamiltonian of solid can be written as

$$\hat{H} = \sum_{i=1}^{Ne} \frac{-\hbar^2}{2m}\nabla_i^2 + \sum_{I=1}^{N_{nuc}} \frac{-\hbar^2}{2M}\nabla_I^2 + \frac{1}{2}\sum_{i\neq j} \frac{e^2}{4\pi\varepsilon_0 \left|\vec{r}_i - \vec{r}_j\right|} - \sum_{i,I} \frac{Z_I e^2}{4\pi\varepsilon_0 \left|\vec{r}_i - \vec{R}_I\right|} + \frac{1}{2}\sum_{I\neq J} \frac{Z_I Z_J e^2}{4\pi\varepsilon_0 \left|\vec{R}_I - \vec{R}_J\right|} \,.$$

The first two terms are the kinetic energy of electrons and nuclei, respectively, and the last three terms refer to the electron-electron, electron-nucleus and nucleus-nucleus interactions. $\hbar = \frac{h}{2\pi}$, m and M are the reduced Planck's constant, electron and nucleus mass, respectively. Z_I is the atomic number of the Ith nucleus, e is the electron charge and $\vec{r}_i$ and $\vec{R}_i$ are symbolized as the positions of the ith electron and Ith nucleus. However, it is practically impossible to solve Eq. (1) for real solid which contains enormous number of electrons and nuclei. This problem however, can be simplified by using the Born-Oppenheimer approximation. In this approximation, the nuclei are treated as stationary and the electrons move around the nuclei. This is because electrons move faster than nuclei for about two orders of magnitude and

hence the kinetic energy of nuclei can be negligible. Moreover, mass of the nuclei is much heavier than that of electron. Consequently, the last term in the Eq. (1) can be set to be constant. The Hamiltonian of solid is reduced to

$$\hat{H} = \sum_{i=1}^{Ne} \frac{-\hbar^2}{2m}\nabla_i^2 + \frac{1}{2}\sum_{i\neq j}\frac{e^2}{4\pi\varepsilon_0\left|\vec{r}_i - \vec{r}_j\right|} - \sum_{i,I}\frac{Z_I e^2}{4\pi\varepsilon_0\left|\vec{r}_i - \vec{R}_I\right|} + \frac{1}{2}\sum_{I\neq J}\frac{Z_I Z_J e^2}{4\pi\varepsilon_0\left|\vec{R}_I - \vec{R}_J\right|}.$$

According to the Born-Oppenheimer approximation, we can explicitly separate the electron and nucleus motion. Hence, the solid wave function can be divided independently into an electron part, $\Psi_e(\vec{r},\vec{R})$ and a nucleus part, $\Psi_N(\vec{R})$, as

$$\Psi(\vec{r},\vec{R}) = \Psi_e(\vec{r},\vec{R})\Psi_N(\vec{R}).$$

The effect from nuclei in electronic problem can be omitted because electron behavior plays an important role in this problem. However, nucleus wave function is able to be added later if our observable properties are related to nuclei. For electrons, the Schrödinger equation can be written as

$$\hat{H}_e\Psi_e(\vec{r},\vec{R}) = E_e\Psi_e(\vec{r},\vec{R}), \tag{2}$$

where

$$\hat{H}_e = \sum_{i=1}^{Ne} \frac{-\hbar^2}{2m}\nabla_i^2 + \frac{1}{2}\sum_{i\neq j}\frac{e^2}{4\pi\varepsilon_0\left|\vec{r}_i - \vec{r}_j\right|} - \sum_{i,I}\frac{Z_I e^2}{4\pi\varepsilon_0\left|\vec{r}_i - \vec{R}_I\right|}.$$

$\Psi_e(\vec{r},\vec{R})$ and E_e are the electron wave function and energy eigenvalue, respectively.

To solve many-electron problem, single electron wave function was initially used for solving Eq. (2). In Hartree theory, many-electron wave function can be obtained from a product of single-electron wave functions. However, this theory fails to understand electronic properties due to violating the antisymmetric property of the wave functions. An improvement from the Hartree theory is the Hartree-Fock (HF) theory. In the HF theory, the HF wave function was proposed as a determinant of single electron wave functions called “Slater determinant”, explicitly including the antisymmetric property of the wave function. Moreover, the exchange interaction is automatically included in the electron Hamiltonian. Although, this theory has various drawbacks, for example, it excludes correlation effects such as screening effects and so on. In addition, this method is not suitable for using with the system containing a large number

of electrons due to consumption of large memory resources and computational expensive as well. From all of these drawbacks, density functional theory (DFT) is presented as an appropriate tool for solving the many-electron problem. The basic idea of DFT is discussed in the next section.

2.2 Density functional Theory

Density functional theory (DFT) has been shown to be a popular method for solving many-electron problems. In principle, this method is an exact method but, in practical, it uses some approximations for exchange-correlation functional. The starting point of this theory comes from the Hohenberg-Kohn theorem [68] consisting of two theorems.

Theorem 1 For any system of interacting particles in an external potential, $V_{ext}(\vec{r})$, there is a one to one correspondence between the external potential and ground state density ($n_0(\vec{r})$). Moreover, the ground state expectation value of any observable quantity *A* is a unique function,

$$\left\langle \Psi \mid \hat{\mathrm{A}} \mid \Psi \right\rangle = \mathrm{A}[n_0(\vec{r})].$$

This theorem implies that the density parameter is the main variable for the DFT instead of the wave function for the HF theory.

Theorem 2 For any external potential applied to an interacting particle system, it is possible to define a universal total energy functional of the particle density, which is written as

$$E[n(\vec{r})] = E_{HK}[n(\vec{r})] + \int V_{ext}(\vec{r}) n(\vec{r}) dr,$$

where $E_{HK}[n(\vec{r})]$ is the universal constant which does not relate to any information of the type of nuclei or their positions. This means that it is represented as an arbitrarily universal constant for the interacting system. However, this constant is still unknown. If knowing this constant, we can determine the ground state energy by minimizing total energy with respect to density by using the variational principle,

$$\left. \frac{\delta E[n(\vec{r})]}{\delta n} \right|_{n=n_0} = 0$$

The exact ground state energy (E_0) corresponding to the ground state density ($n_0(\vec{r})$) is given by

$$E_0 = E[n_0(\vec{r})]$$

According to the above theorems, the density is used as a primary quantity for calculating all observable quantities. Kohn and Sham [69] proposed a new Schrödinger-like equation, called "Kohn-Sham equation", as a function of the density in 1965. Moreover, this equation maps an interacting system to a fictitious non-interacting system in which the particles moving in an effective field (V_{eff}). The energy functional in the DFT can be written as

$$E[n(\vec{r})] = T_0[n(\vec{r})] + \frac{1}{2}\iint \frac{n(\vec{r})n(\vec{r}^{\,/})}{\left|\vec{r}-\vec{r}^{\,/}\right|} d\vec{r}\,d\vec{r}^{\,/} + \int V_{ext} n(\vec{r})\,d\vec{r} + E_{xc}[n(\vec{r})]. \quad (3)$$

The first, second, third and fourth terms of Eq. (3) are the non-interacting kinetic energy functional $(T_0[n(\vec{r})])$, the electron-electron interaction energy or Hatree energy, the external potential energy due to nuclei and exchange-correlation energy, respectively. By minimizing of Eq. (3) with respect to the density, the Kohn-Sham equation (in atomic unit) can be obtained as

$$\left(-\frac{\nabla_i^2}{2} + V_{eff}(\vec{r})\right)\Psi_i(\vec{r}) = E_i\Psi_i(\vec{r}) \quad (4)$$

where the effective potential is given by

$$V_{eff}(\vec{r}) = V_{ext}(\vec{r}) + \int \frac{n(\vec{r})}{\left|\vec{r}-\vec{r}^{\,/}\right|} d\vec{r}^{\,/} + V_{xc}[n(\vec{r})] \quad (5)$$

with $V_{xc}[n(\vec{r})] = \frac{\delta E_{xc}}{\delta n}$. $\Psi_i(\mathbf{r})$ is the Kohn-Sham orbital which is not the wave function of the system but the density obtained from the Kohn-Sham orbitals is the exact density as the true system. To solve the Kohn-Sham equation, algorithm for solving the self-consistent Kohn-Sham equation is well described in Figure 2.1. First, the density is initially guessed and then the effective potential functional (Eq. (5)) is calculated from the guessed density. Next, the Kohn-Sham equation is solved in order to get the total energies and the Kohn-Sham orbitals. After that the new density can be obtained from the calculated Kohn-Sham orbitals and is used as the initial density for the next step. This process runs self-consistently until the convergence of density is reached. Finally, the output quantities are calculated via the converged density.

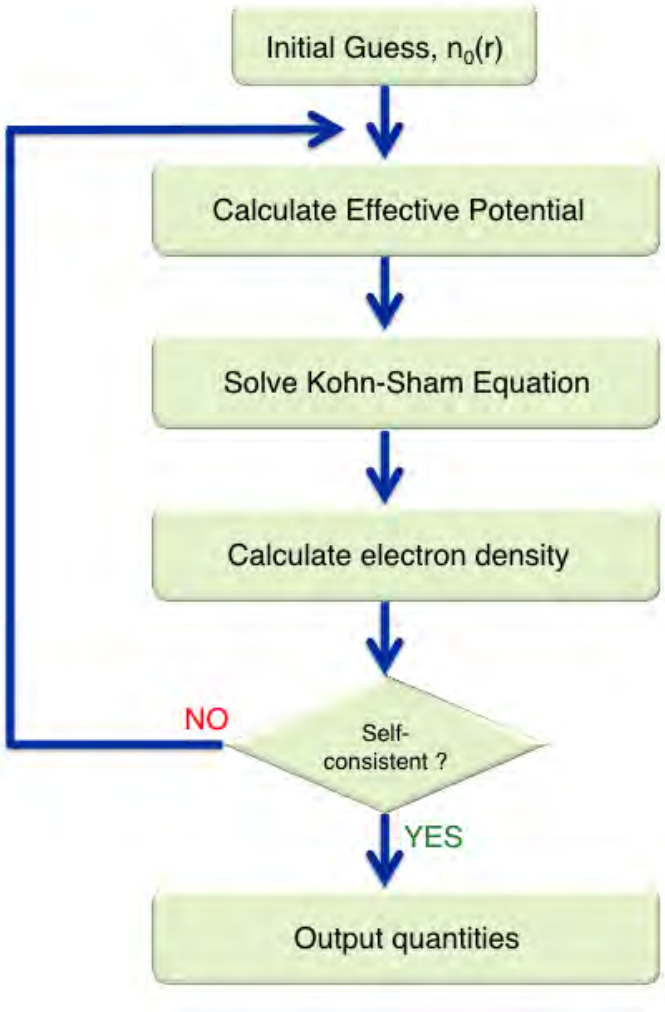

Figure 2.1 schematic methods for solving self-consistent Kohn-Sham equation [70].

According to Eq.(5), the first two terms of the effective potential can be exactly evaluated where the last term ($V_{XC}[n(\mathbf{r})]$) is still unknown. The $V_{XC}[n(\mathbf{r})]$ contains all unknown terms i.e. many body effect of kinetic energy, correlation effects, etc. Based on the conventional exchange-correlation functional, two types of E_{xc}, namely the Local Density Approximation (LDA) and Generalized Gradient Approximation (GGA) are considered. The exchange-correlation functional can be expressed as

$$E_{xc}[n(\vec{r})] = \int \varepsilon_{xc}[n(\vec{r})]n(\vec{r})dr,$$

where $\varepsilon_{xc}[n(\vec{r})]$ is exchange-correlation density corresponding to the density n(**r**). In the LDA scheme, the exchange-correlation functional is derived from the homogeneous interacting

electron gas. It works very well for slow varying density system, for instance, free electron-like system. Moreover, it can well describe for some other systems i.e. semiconductors and insulators. In metal organic framework-5 and covalent organic framework-1, they can be surprisingly reproduced the correct trends of the hydrogen adsorption energies obtained from experiment and Møller-Plesset perturbation theory, whereas other exchange-correlation functionals fail to predict the correct trend of hydrogen physisorption energies [27, 67]. However, the electron density in real systems is no longer homogeneous and hence the LDA scheme will be not well described in many cases. There are however, many attempts to improve the LDA by including higher-order terms of the exchange-correlation energy. In the GGA, the exchange-correlation energy contains information from both density and gradient of density (∇n). By using this idea, many types of GGA functional have been created such as Perdew-Wang 91 and Perdew-Burke-Ernzerhof. In principle, the GGA potential should give a better result compared to LDA because it contains more information of the electron density. However, in practice, it is not always true that the GGA gives a better result than the LDA. Currently, there is no exchange correlation functional which is suitable for all systems. Hence we need to carefully check which functional gives the reasonable results compared to experimental data (or high accuracy methods) before performing the calculations.

- **Binding Energy**

In order to know how strong interaction between adsorbent and absorber, the binding energy needs to be determined. For the arbitrary system consisting of adsorbent trapped on the surface of host material, the binding energy (ΔE) between the former and the latter are calculated by

$$\Delta E = E(\text{host}) + E(\text{Ads}) - E(\text{host:Ads}),$$

Where $E(\text{host})$, $E(\text{Ads})$, and $E(\text{host:Ads})$ stand for total energy of host material, adsorbent and adsorbent trapped on the surface of host material, respectively. Usually, the total energy can be obtained from the DFT calculation. By applying this idea to evaluate the metal M adsorbed in the host material. The metal binding energy (ΔE_M) is given by

$$\Delta E_M = E(\text{host}) + E(M) - E(\text{host:M}),$$

Similarly, for the hydrogen adsorption energy or ΔE_{H2} , it is calculated by the following equation,

$$\Delta E_{H2} = E(\text{host}) + E(H_2) - E(\text{host}{:}H_2).$$

$E(H_2)$ is the total energy of isolated H_2 molecule.

2.3 Born-Oppenheimer Molecular Dynamics

In condensed matter physics, molecular dynamics simulation (MD) is a very important tool to understand the dynamical properties of materials at a particular temperature. It can be used for calculating the time-dependent quantities of materials such as mean square displacement, radial distribution function, etc. Molecular dynamics simulation is a method to solve time evolution of particles or nuclei in the solid or liquid (or even gaseous) phase by numerically solving an equation of motion, Newton's equation of motion in this case. In classical MD (CMD), classical forces acting on each nucleus can be determined from an empirical potential, e.g. Finnis-Sinclair [71], Lennard-Jones or 6-12 and Tersoff [72]. For large systems, the speed of the CMD simulations is very fast but the accuracy of these simulations is still problematic due to inability to study the breaking and forming of chemical bonds. However, this problem can be solved by using quantum molecular dynamics (QMD). In this section, we only considered Born-Oppenheimer Molecular Dynamics (BOMD). For the BOMD, the electronic force acting on each nuclei is obtained from first-principles calculations such as density functional theory calculations. The nucleus motions must obey the second law of Newton's equation of motion when time is evolved.

$$\vec{F}_i = -\vec{\nabla} E_i = m_i \frac{d^2 \vec{r}_i}{dt^2}$$

where $\vec{F}_i$ and E_i stand for the forces acting on the i^{th} nucleus and energy functional obtained from the *ab initio* calculations, respectively. m_i is mass of the i^{th} nuclei and $\vec{r}_i$ is the position of the i^{th} nucleus. However, the BOMD calculations are computationally expensive and limited to small systems, usually containing less than a few hundreds of atoms. To determine the amount of ion trapped around one reference atom, the radial distribution function needs to be calculated. Detail description of the radial distribution function is discussed below.

- **Radial distribution function**

The radial distribution function (RDF or g(r)) can be obtained from molecular dynamics simulations, X-ray and neutron scattering experiments. It is used for probing the local configuration of the system of interest and defined by

$$g(r) = \frac{N_i(r)}{4\pi\rho r^2 dr}.$$

$N_i(r)$ and ρ stand for total number of atoms inside spherical shell with radius larger than r and smaller than r+dr and the average density of the system, respectively. In addition, it will converge to 1 when r approaches infinity. The coordination number or number of nearest neighbors (N) around the reference atom can be given by

$$N = \int g(r)dr.$$

.

CHAPTER III

Results and Discussion

In this chapter, we divided all results related to this project into three sections as discussed below.

3.1 Covalent Triazine based Framework -1

A new material called Covalent Triazine-based Framework-1 (CTF-N) was successfully synthesized [44-46]. CTF-N is thermally stable up to about 600 ^{o}C [44]. Its surface area, measured using nitrogen sorption experiments, is 791 m^2/g. The crystal structure of the CTF-N possesses space group P6/mmm. The lattice parameters of this structure are a = b = 14.574 Å and c = 3.4 Å [44]. The crystal structure of the CTF-N consists of a triazine ring (C_3N_3) covalently bonded with phenyl rings forming a periodic framework. The unit cell of the CTF-N contains 42 atoms consisting of 24 C atoms, 6 N atoms and 12 H atoms. The crystal structure of CTF-N is shown in Figure 3.1.

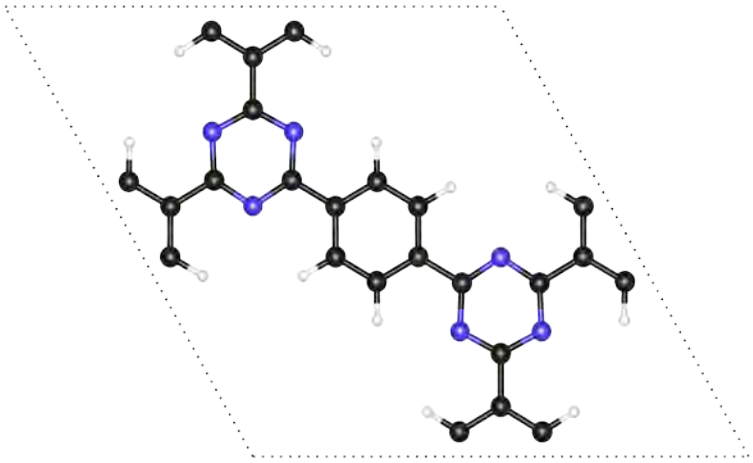

Figure 3.1 Crystal structure of the CTF-N. Nitrogen, carbon, and hydrogen atoms are shown as blue, black, and white spheres, respectively. Black dots represent the unit cell of the CTF-N.

According to calculated results from Zhu and Meunier [74], they carried out the electronic structure of CTF-N system by using density functional theory (DFT) with a Perdew–Burke–Ernzerhof exchange correlation functional [74]. It was found that CTF-N is a wide band

gap semiconductor with a 2.65 eV energy gap. Moreover, they also investigated addition of 2–4 phenyl rings between the triazine rings. Their results showed that the energy gaps decreased when the number of inserted phenyl rings was increased. Kuhn *et al.* [44] investigated the pore size distribution evaluated using a nonlocal DFT (NLDFT) technique. They found that the pore size of CTF-N was 1.2 nm.

In this work, the energy gap of the CTF-N was determined by means of density functional theory. We also studied replacement of all N atoms in the triazine ring with either P, As or Sb. These structures are referred to as CTF-P, CTF-As and CTF-Sb, respectively. The optical band gaps of the CTF-NM (NM = N, P, As and Sb) were determined. Finally, the relationship between the energy gaps and various concentrations of P and As in CTF-N was investigated.

Structural parameters of CTF-N were determined by optimization with no symmetry constraint. Moreover, other structures were relaxed, e.g., CTF-P, CTF-As and CTF-Sb. P, As and Sb atoms were chosen as replacements for N in CTF-N because they have identical charge states with different atomic sizes, i.e., 0.65, 1.00, 1.15 and 1.45 Å for N, P, As and Sb, respectively [75]. The structural parameters of CTF-NM (NM = N, P, As and Sb) systems are presented in Figure 3.2.

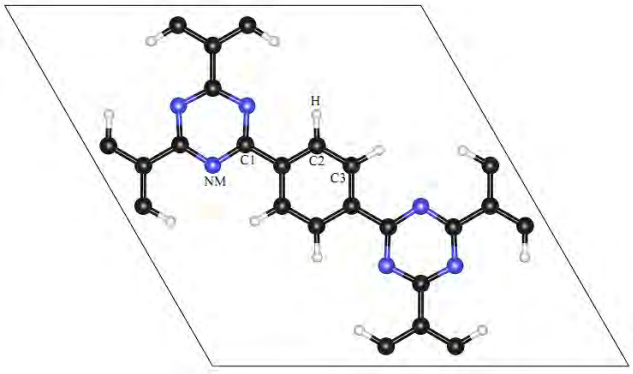

CTF-NM	NM-C1-NM (°)	NM-C1 (Å)	C2-C3 (Å)	C3-H (Å)
CTF-N	124.872	1.345	1.405	1.087
CTF-P	130.391	1.750	1.404	1.089
CTF-As	131.150	1.882	1.405	1.089
CTF-Sb	131.188	2.122	1.415	1.090
CTF-N (exp)[44]	124.385	1.350	1.396	1.085

Figure 3.2 Optimized structural parameters of CTF-NM (NM = N, P, As and Sb). Positions of the NM, C1–C3 and H atoms are presented in the image on the left of the table.

As clearly seen in Figure 3.2, the structural parameters of the CTF-N obtained are in excellent agreement with reported experimental values [44]. For the CTF-P, CTF-As and CTF-Sb systems, the C2–C3 and C3–H distances in Figure 3.2 are unchanged, whereas the NM–C1 distances and the NM–C1–NM bond angles of the CTF-P, CTFAs and CTF-Sb are seen to be

significantly altered from those of CTF-N. Replacement of N with nonmetal atoms such as P, As and Sb in CTF-N changes only the molecular structure of the NM_3C_3 ring without affecting of the phenyl rings during substitution of N with larger atoms in the CTF-N. Next, electronic density of states of CTF-NM (NM = N, P, As and Sb) were determined. The corresponding density of states is shown in Figure 3.3.

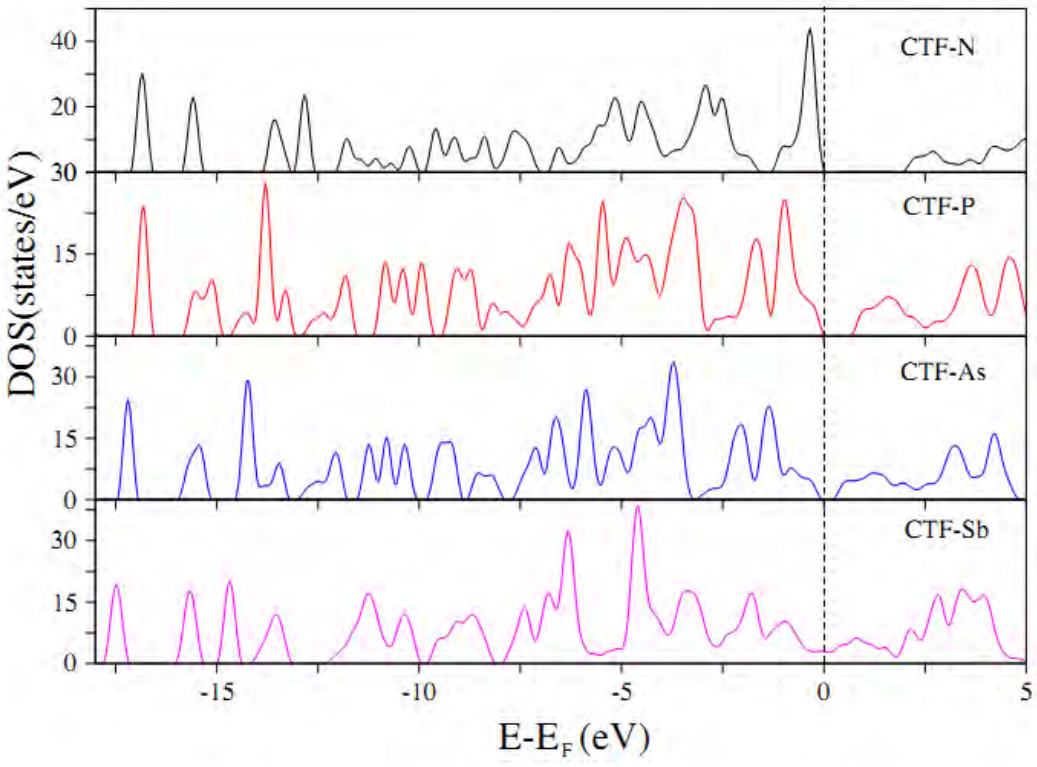

Figure 3.3 Electronic density of states of the CTF-N, CTF-P, CTF-As and CTF-Sb. The dotted vertical line represents the Fermi level.

According to Figure 3.3, it can also be seen that the energy gaps (E_g) are 2.02, 0.69, 0.22 and 0 eV for CTF-N, CTF-P, CTF-As, and CTF-Sb, respectively. The E_g found are in good agreement to those determined by Zhu and Meunier [74]. The trend of optical band gaps in these considered structures was found to decrease as the covalent radius was increased. As seen in Figure 3.3, the lowest unoccupied states (lowest energy states of the conduction band) approach to the Fermi level when we replace N in the CTF-N with larger atoms. This resulted in reducing the optical band gap. To understand the reduction of the optical band gap when larger metals are replaced with N, the partial density of states of the CTF-N states was determined as shown in Figure 3.4.

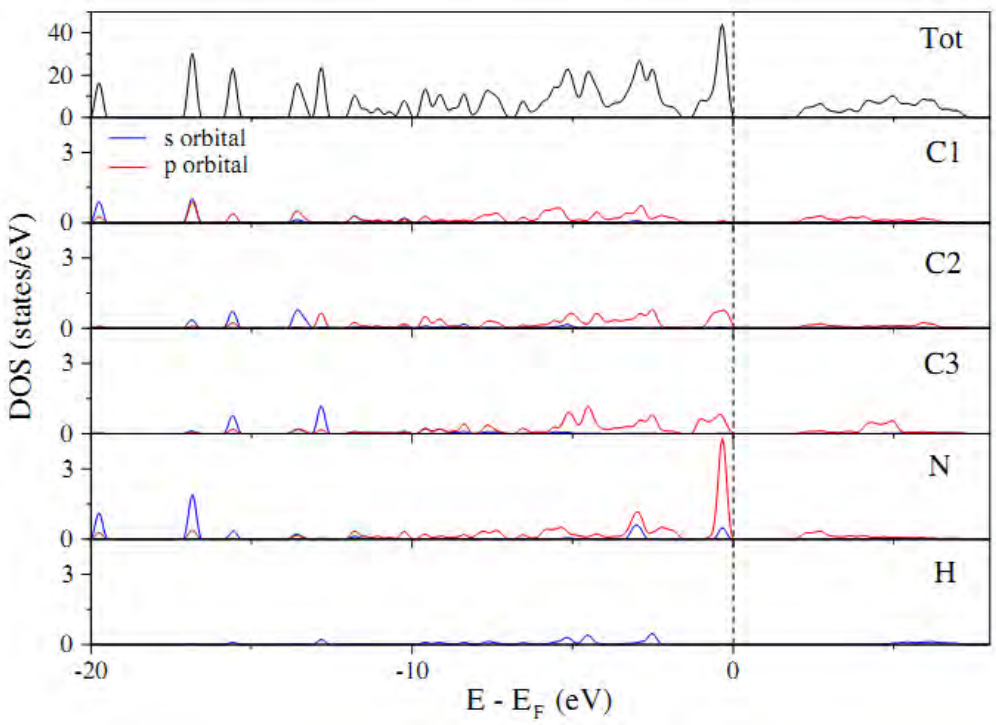

Figure 3.4 Total density of states and the partial density of states of N, C1, C2, C3, and H atoms in the CTF-N. The positions of N, C1–C3 and H atoms are presented in Figure 3.2.

According to the partial density of states data, the first peak above the Fermi level primarily comes from the p states of N atoms of the triazine ring. This clearly shows that p states of nonmetal atoms e.g., P, As and Sb, lead to lower the energy gap seen in Figure. 3.3. Another reason for the reduction of optical band gaps is that replacing N with larger nonmetals in the triazine ring (see Figure. 3.3) might be from slight distortion of the NM_3C_3 ring. As a consequence, the electronic structures of the CTF-P, CTF-As and CTF-Sb were slightly changed from the intrinsic CTF-N. As shown in Figure 3.3, the band gap can be altered by substituting all N atoms in the triazine ring with either P, As or Sb. Based on this result, changing concentrations of N in the CTF-N with the atoms having equal valence electrons but different atomic sizes can change the optical band gap. In the current work, the concentrations of P and As in the CTF-N were changed by partially replacing N atoms with either P or As. The relationship between the optical band gap and concentrations of P and As in the CTF-N is shown in Figure 3.5. Our results reveal that the energy gap exhibited a non-linear drop when P and As concentrations were increased. Moreover, varying Sb concentrations in the CTF-N was considered.

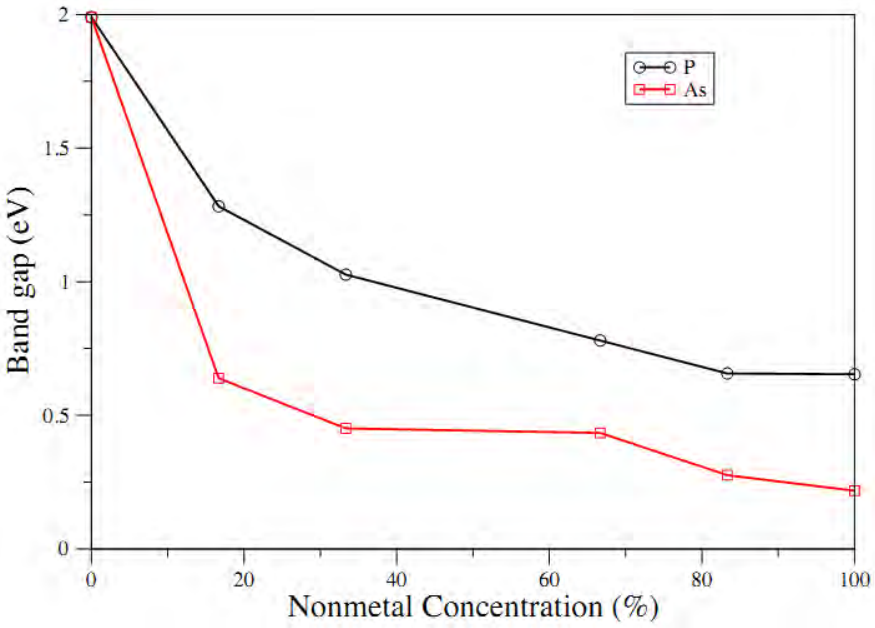

Figure 3.5 Non-linear relationships between energy gap and various concentrations of P and As in CTF-N.

Unfortunately, metallic behavior was observed when Sb replaced N in the CTF-N. This is likely caused by the existence of Sb p states near the Fermi level causing the optical band gap to vanish. The relationship between the optical band gap and concentrations of both P and As was fitted with a third-order polynomial form as presented below.

$$E_{g,P} = -3.09\times10^{-6}c_P^3 + 6.71\times10^{-4}c_P^2 - 0.05c_P + 2.02$$

$$E_{g,As} = -8.91\times10^{-6}c_{As}^3 + 1.67\times10^{-3}c_{As}^2 - 0.10c_{As} + 2.02$$

where $E_{g,P}$ and $E_{g,As}$ stand for the optical band gap of the CTF-N with various P and As concentrations, respectively. Concentrations of P and As are symbolized as c_P and c_{As}, respectively. Based on these results, it is possible to tune the optical band gap by changing the electronic structure of the materials. In addition, increasing concentrations of P and As in the CTF-N yields nonlinear behavior of the optical band gap. Finally, these findings can stimulate both theorists and experimentalists to apply this method to tune the optical band gap of appropriate materials for their use in other optical applications.

3.2 Covalent Organic Framework-366

A new class of porphyrin based material, named covalent organic framework-366 (COF-366), was successfully synthesized [76]. The unit cell of COF-366 possesses a P4/m space group

with lattice parameters of a = b = 25.696 Å and c = 12.541 Å [76]. Its unit cell contains 212 atoms consisting of 120 C atoms, 16 N atoms and 76 H atoms. Moreover, the crystal density and BET surface area of COF-366 are 0.36 g/cm^3 and 735 m^2/g, respectively [76]. The COF-366 crystal structure forms an AA stacking sequence. It has a pore size of 20 Å and an AA interlayer distance of 6.27 Å [76]. Each layer contains tetra(p-amino-phenyl) porphyrin (TAPP) bonded with a terephthaldehyde chain to form the periodic framework as shown in Figure 3.6

.

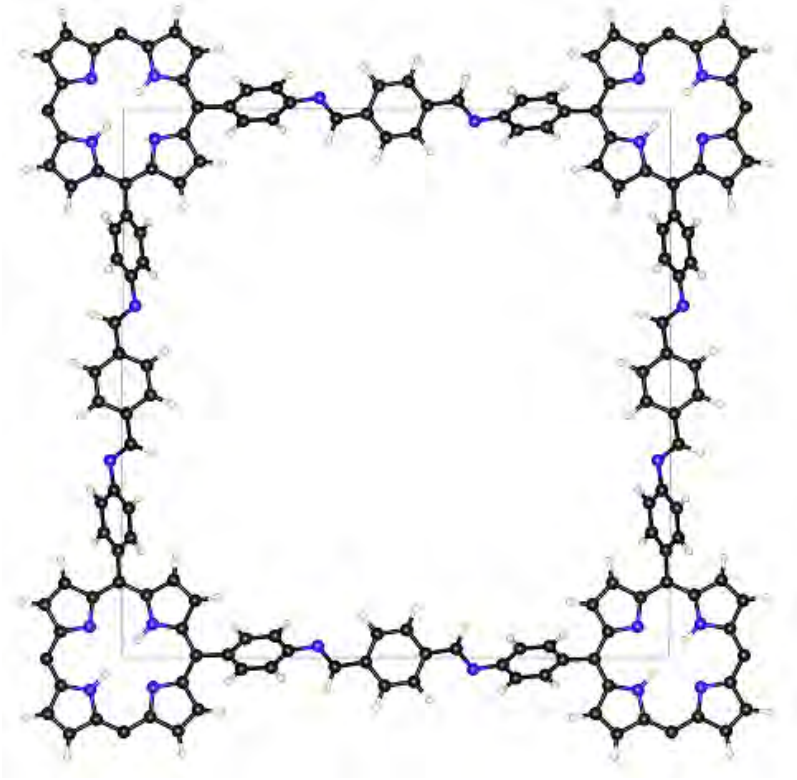

Figure 3.6 The primitive cell of COF-366. Blue, black and white spheres are symbolized by N, C and H, respectively. Black line is the unit cell of the COF-366.

In the present work, we theoretically studied the hydrogen adsorption properties of Li decorated COF-366. In addition, the hydrogen capacities of Li functionalized COF-366 at three different temperatures, 77 K, 150 K and 300 K, were evaluated.

First, geometry optimization with no symmetry constraints was applied to COF-366. We found that our structural parameters after optimization differ from experimental data by less than 3%. It was found that a = 25.493 Å, b= 25.488 Å and c = 12.144 Å from our calculation. Experimentally determined values were a = b = 25.696 Å and c = 12.541 Å [76]. Hence, our computations and experimental results are in excellent agreement.

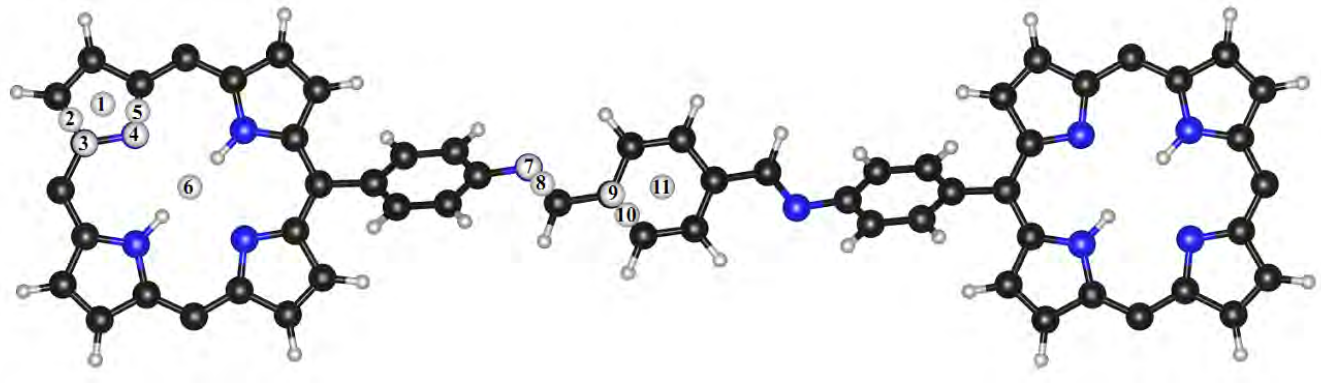

Figure 3.7 Locations of Li adsorption sites in the COF-366. For the adsorption sites on the TAPP, Li can be trapped at center of pentagon ring, C--C bridge, onC, onN, N-C bridge and center site denoted by site numbers 1-6. Numbers 7-11 are the onN, N-C bridge, onC, C-C bridge and hollow sites for the adsorption sites on the terephthaldehyde chain, respectively.

Then, Li atoms were placed at all possible adsorption sites on COF-366. According to COF-366 crystal geometry, Li atoms can be trapped on both the TAPP and terephthaldehyde chain. On the TAPP, Li atoms can be placed at several locations. These include the center of the pentagon, C-C bridge, onC, onN, N-C bridge of the pentagon ring and at the center of the TAPP. These appear as sites 1-6 in Figure 3.7, respectively. Additionally, the positions of Li adsorption sites on the terephthaldehyde chain are the onN, N-C bridge, onC, C-C bridge and hollow sites as shown by sites 7-11 in Figure 3.7. To evaluate the strength of Li interactions to COF-366, Li binding energy (ΔE_{Li}) was determined. It was calculated by

$$\Delta E_{Li} = E(\text{COF-366}) + E(\text{Li}) - E(\text{COF-366:Li}),$$

where $E(\text{COF-366:Li})$, $E(\text{COF-366})$ are the total energies of COF- 366 with and without Li decorations. The total energy of isolated Li atom is represented as $E(\text{Li})$. Based on our Li binding energy calculations, we found that the center site (site 6 in Figure. 3.7) is the most preferable Li adsorption site for Li binding on the TAPP ring. On the terephthaldehyde chain, the onN site (site 7 in Figure 3.7) is the most stable adsorption site for Li. The Li binding energies of these two sites were found to be 2.97 eV for the center site and 2.34 eV for the onN site.

Next, various hydrogen loadings ranging from 1 to $3H_2$ molecules were placed on Li atoms which were trapped at these adsorption sites. The hydrogen adsorption energy can be calculated by the following:

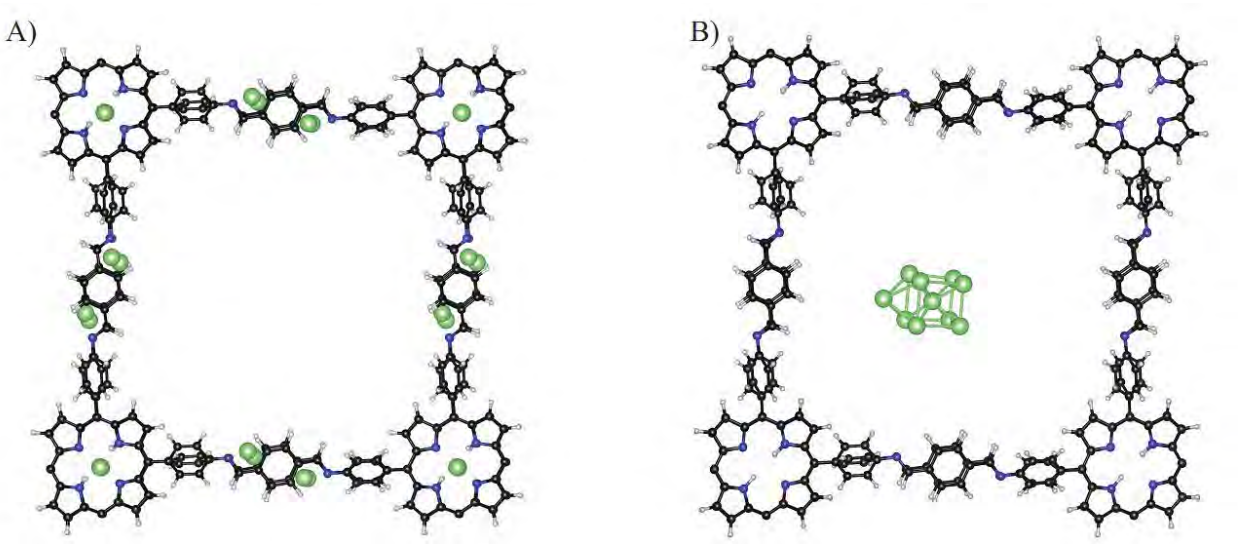

Figure 3.8 Optimized crystal structures of (A) 10 Li atoms trapped on the COF-366 surface, (B) 10 Li atoms formed as a cluster at center of the COF-366 pore. Li, C, N and H are represented as green, black, blue and white spheres, respectively.

$$\Delta E_{H_2} = E(\text{COF-366:Li}) + E(H_2) - E(\text{COF-366:Li+nH}_2),$$

where $E(\text{COF-366:Li+nH}_2)$ and $E(H_2)$ are the total energies of nH_2 molecules adsorbed on Li decorated COF-366 and the total energy of a free H_2 molecule, respectively. For a Li atom trapped at the center site, we found that the hydrogen binding energies per H_2 for 1-3 H_2 molecules were 0.13, 0.08 and 0.06 eV, respectively. In addition, the hydrogen adsorption energies per H_2 were 0.22, 0.12 and 0.03 eV when 1-3 H_2 molecules were trapped on Li adsorbed at the onN site. To understand the interaction between Li atoms and adsorbed hydrogen molecules, Bader charge analysis [77] was done for the above cases. Our results showed that 0.9e from a Li atom were transferred to COF-366. Hence, the interaction between H_2 molecules and Li atom is governed primarily by charge-quadruple interaction. These results are excellent agreement with previous works [21, 78]. Next, several Li atoms were simultaneously placed at the center and onN sites of COF-366. However, it was necessary to determine if Li atoms prefer either trapping on the COF-366's surface (Figure 3.8 A) or form as a Li cluster at center of the COF- 366 pore (Figure 3.8 B). This leads us to perform total energy calculations for these two cases. In Figure 3.8 A, we placed 10 Li per unit cell, namely 8 Li at the onN site and 2 Li at the center site. Description of these adsorption sites is shown

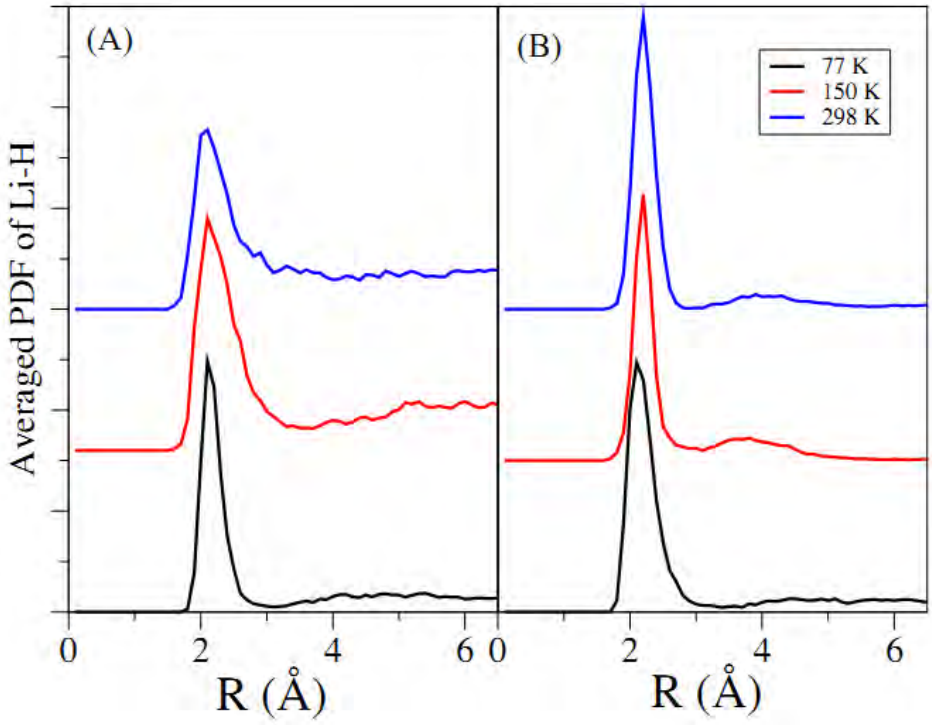

Figure 3.9 The averaged pair distribution functions and distance between Li and hydrogen atoms (R) for the cases of (A) Li trapped at center site and (B) Li adsorbed at the onN.

graphically in Figure 3.7. It was found that total energy of Li decorations on the COF-366 surface was lower than that of Li clustered at the center of the COF-366 pore by approximately 1.1 eV/Li atom. In other words, 10 Li atoms are unlikely to form as a cluster at the center of the COF-366 pore. These results are in good agreement with those of both Blomqvist et al. [21] and Sun et al. [79]. To investigate hydrogen uptake of the Li functionalized COF-366 system, a total of 30H_2 molecules (3 H_2 molecules on each Li atom) were placed on Li decorated COF- 366 as an initial configuration. We then preformed *ab initio* molecular dynamics simulations at ambient pressure and temperatures of 77, 150, and 298 K. The 2 fs time step was used in all molecular dynamics calculations. For each temperature, the pair distribution function (PDF) between Li and hydrogen atom was determined. In the present work, the PDFs were averaged over 10 ps at thermodynamic equilibrium for all considered temperatures as shown in Figure 3.9. According to this Figure, the number of hydrogen atoms adsorbed by Li at each temperature can be obtained by integrating the PDF over the first peak. At 77 K, we found that 3.50 H atoms and 4.01 H atoms are trapped on Li when Li was decorated at the center and onN sites, respectively. By increasing the temperature to 150 K, 2.37 H and 3.14 H can bind with Li atom adsorbed at center and onN sites, respectively. At room temperature, only 1.72 H was able to

bind on Li atom trapped at center site. For Li adsorbed at the onN site, it was found that 2.03 H could be trapped on a Li atom. Based on these results, the hydrogen capacities could be calculated. The results showed that hydrogen uptakes at ambient pressure and temperatures of 77, 150, and 298 K were 2.06, 1.58, and 1.05 wt%, respectively. In comparison to experimental data of Yaghi [80], it is clearly shown that the hydrogen capacity of Li doped COF-366 is about 2 times higher than that of pristine COF-366. Hence, it can be seen that enhancement of hydrogen capacity came from Li doping. Usually, hydrogen uptake by various high surface area materials at 77 K and ambient pressure is less than 2.0 wt%. For example, it is below 1.5 wt% for most of covalent organic frameworks [81, 82] and 2.0 wt% for Isoreticular metal-organic frameworks [22, 24]. However, the hydrogen capacity reported by us is still lower than some other systems, e.g., UTSA-20 [83] and Li functionalized Phthalocyanine Covalent Organic Frameworks [84]. Based upon the amount of hydrogen adsorbed on Li decorated COF-366, the volumetric hydrogen uptake can also be calculated. We found that they are 8.90, 6.80 and 4.48 g/L for 77, 150 and 298 K, respectively. The volumetric density of Li decorated COF-366 is indeed low owing to rather large unit cell volume. To make the hydrogen capacity of these materials as high as possible, the host material should be as light as possible. At the same time, it needs to bind a great number of hydrogen molecules. For metal decoration on high surface area materials, Li is a good candidate as a decorating metal for hydrogen storage purposes. This is due to its light weight and rather high interaction energy between hydrogen molecules and host material. Lastly, we propose that functionalization of Li atoms onto a suitable host might be a good strategy to reach the DOE target.

3.3 Zeolitic Imidazolate Framework-23

Zeolitic imidazolate frameworks (ZIFs) are new classes of high-surface area materials, successfully synthesized by Yaghi's research group [57, 85]. As shown by Banerjee et al. [85] both pore size and surface area of these materials can be tuned by adjustment the metal nitride (MN_4) unit (M=Zn, Co, Cu) and imidazole ligands. Consequently, the ZIFs can be used in various applications such as catalyst [86], biosensor [87], gas storage media e.g. N_2 [88], CO_2 [88, 89] and CH_4 [88]. Based on both theoretical and experimental studies [59, 90], ZIFs show great promise of hydrogen storage materials. According to neutron diffraction experiments at 30 K and ambient pressure [59], ZIF-8 can trap 28 hydrogen molecules corresponding to 4.2 H_2 wt%. By increasing the temperature to 77 K and 1 bar of pressure, the hydrogen capacity is dramatically

decreased to 1.3 wt% [91]. Based on the grand canonical Monte Carlo simulations, ZIF-11 can uptake hydrogen about 3.96 wt% at 77 K and 100 bar. When the pressure is reduced to 1 bar, the hydrogen uptake is slightly dropped to 2.39 wt% [90]. For Zeolitic imidazolate framework-23 (ZIF-23), there is no report in the literature related to the hydrogen adsorption. Thus this motivates us to investigate the hydrogen adsorption properties of this system. For ZIF-23 or Zn-ZIF23 system, it consists of tetrahedral cluster of ZnN_4 covalently bonded to the 4-Azabenzimidazolate as an organic linker. Its unit cell contains 108 atoms consisting of 4 Zn atoms, 24 N atoms, 48 C atoms and 32 H atoms. The crystal structure of the ZIF-23 is an orthorhombic crystal system with space group P212121. The lattice constants are a = 9.5477 Å, b = 10.1461 Å and c = 12.4459 Å. Its crystal density is 1.662 g/cm^3 [57]. In the present work, we investigated the structural parameters and the hydrogen adsorption energies of Be-, Zn- and Cd-based ZIF23 structures, referred to in the following as Be-ZIF23, Zn-ZIF23 and Cd-ZIF23. The crystal structure of the M-ZIF23 (M= Be, Zn, and Cd) are shown in Figure 3.10

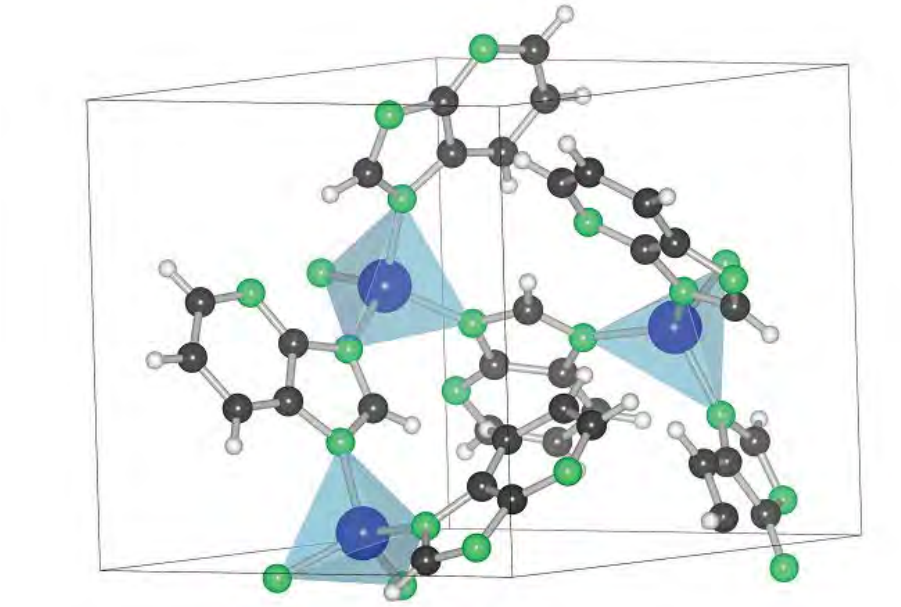

Figure 3.10 Crystal structure of the M-ZIF23 (M = Be, Zn and Cd). M, N, C and H atoms are denoted by blue, green, black and white spheres, respectively. The solid line represents the unit cell of the M-ZIF23.

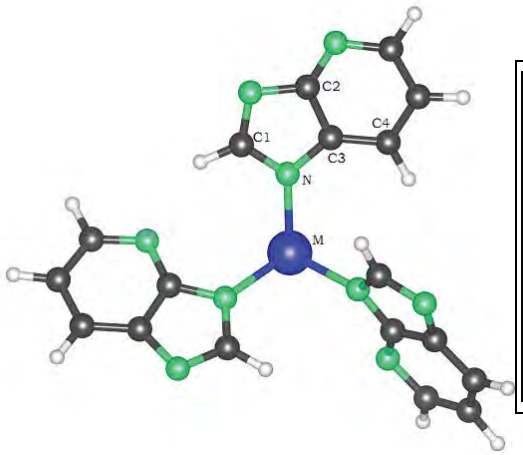

M-ZIF23	M-N (Å)	N-M-N (°)	N-C1 (Å)	C2-C3 (Å)	C3-C4 (Å)
Be-ZIF23	1.79	109.49	1.36	1.42	1.40
Zn-ZIF23	2.05	109.45	1.35	1.42	1.40
Cd-ZIF23	2.25	109.20	1.35	1.42	1.40
Zn-ZIF23 (exp)[57]	2.01	109.00	1.34	-	1.39

Figure 3.11 Structural parameters of M-ZIF23 (M = Be, Zn and Cd) after performing structural optimization. Positions of M, N, C1–C4 are presented at picture on the left hand side.

3.3.1 Structural Parameters of the Be-, Zn- and Cd-ZIF23

First, the Be-, Zn- and Cd-ZIF23 were fully relaxed by discarding the symmetry constraint. The structural parameters after optimization are listed in Figure 3.11. According to Figure 3.11, it is clearly seen that the structural parameters of the Zn-ZIF23 are in excellent agreement with the experimental data [57]. Hence, our calculation results are rather accurate. By considering ionic radius of Be, Zn and Cd, the atomic size of Cd is the largest followed by Zn and Be. The ionic radii of Be, Zn and Cd are 0.59, 0.88 and 1.09 Å respectively. As shown in Figure 3.11, our results revealed that the N–C1, C2–C3 and C3–C4 distances are unchanged, whereas M–N distances of these structures are increased when atomic size of M atoms is gained. This leads to the fact that there is no any effect to the imidazole ring due to the different in size of M atoms at the tetrahedral cluster. Moreover, we found that the M–N distances are increased resulting in improvement of the electric dipole moment when size of M in metal nitride cluster is gained. Based on these results, the electric dipole moment of Cd-ZIF23 is the highest followed by Zn-ZIF23 and Be-ZIF23.

3.3.2 Hydrogen Adsorption of the Be-, Zn- and Cd-ZIF23

In this section, we placed single hydrogen molecule at various adsorption sites of M-ZIF23 structures and then investigated the hydrogen adsorption energies of these structures. We firstly considered the adsorption sites of Zn-ZIF23. Based on the crystal geometry of the Zn-ZIF23, we can divide the adsorption sites into two different parts, namely the adsorption sites

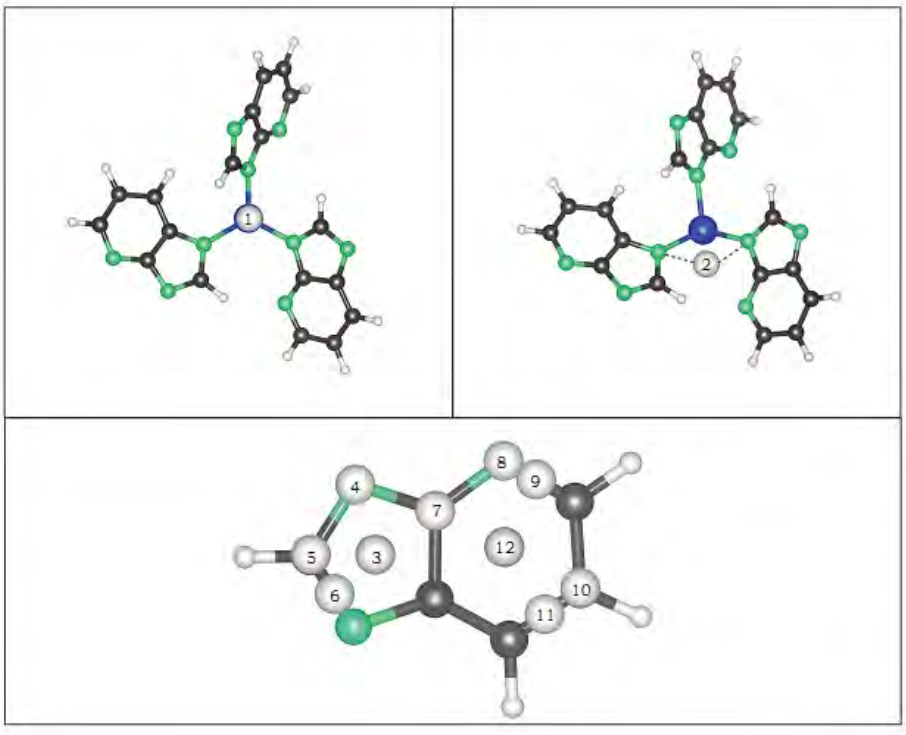

Figure 3.12 Hydrogen adsorption sites of the M-ZIF23 (M = Be, Zn and Cd). Blue, green, black and white spheres are represented as M, N, C and H, respectively

near tetrahedral ZnN_4 cluster and on the 4-Azabenzimidazolate ligand. The adsorption sites near the ZnN_4 cluster consists of two locations, namely ZnN_3 and ZnN_2 as labeled by sites number 1 and 2 in Figure 3.12. Moreover, there are 10 different hydrogen adsorption sites on the organic ligand considered in the present work. For the pentagon ring of carbon in the organic ligand, hydrogen molecule can trap at center of the pentagon rings (number 3), top of N (number 4), top of C (number 5), C–C bridge (number 6), top of C connected to hexagon ring (number 7). In addition, there are 5 different adsorption sites on the hexagon ring of the organic ligand represented by the sites number 8–12 in Figure 3.12.

To investigate the interaction between hydrogen molecule and the Zn-ZIF23, the hydrogen binding energy at a particular adsorption site is determined. It can be given by

$$\Delta E_{H_2} = E(\text{Zn-ZIF23}) + E(\text{H}_2) - E(\text{Zn-ZIF23:H}_2),$$

where $E(\text{Zn-ZIF23})$ and $E(\text{H}_2)$ stand for total energy of isolated Zn-ZIF23 and H_2 molecule, respectively. $E(\text{Zn-ZIF23:H}_2)$ is total energy of single hydrogen molecule adsorbed on the Zn-ZIF23 structure. According to above equation, the positive ΔE_{H_2} implies that hydrogen molecule can adsorb on the Zn-ZIF23 host. In contrast, the hydrogen molecule is unable to

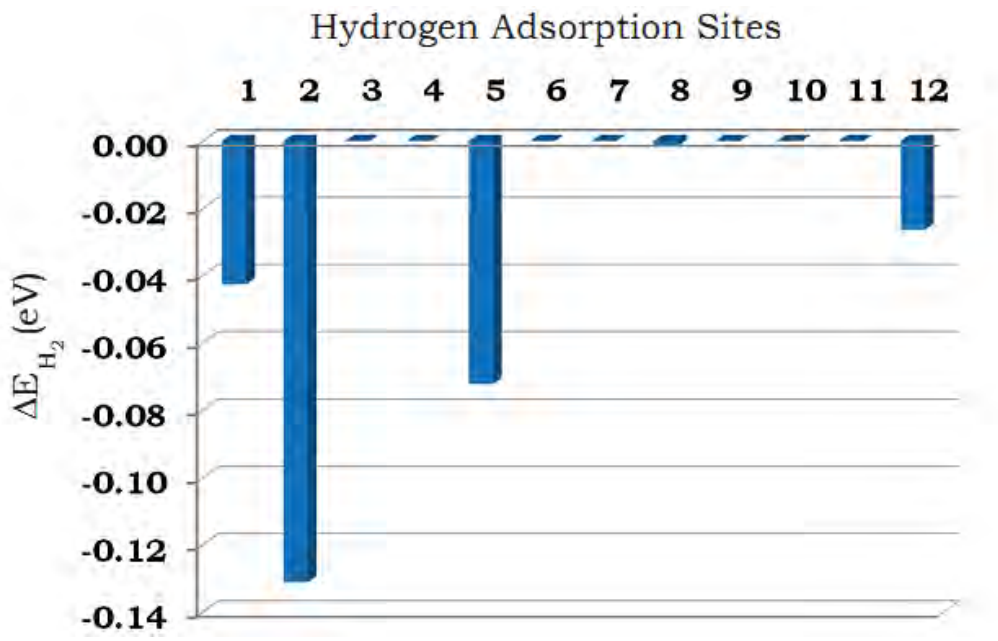

Figure 3.13 Hydrogen adsorption energies of the Zn-ZIF23 at 12 different adsorption sites. The numbers of adsorption sites shown here are referred to the number of adsorption sites in Figure 3.12. We would like to note that hydrogen can bind to the Zn-ZIF23 leads to positive value of ΔE_{H_2}. On the other hand, hydrogen molecule does not bind with the Zn-ZIF23 host when ΔE_{H_2} is negative value. For the unstable adsorption sites, the hydrogen adsorption energy is set to be zero.

trap on the Zn-ZIF23 host leading to the negative value of ΔE_{H_2}. The calculated hydrogen adsorption energies of the Zn-ZIF23 at 12 different sites are displayed in Figure 3.13.

As clearly seen in Figure 3.13, the hydrogen binding energies at ZnN_2 and ZnN_3 adsorption sites are -131.16 and -42.59 meV, respectively. By considering the adsorption sites on the 4-Azabenzimidazolate ligand, the hydrogen adsorption energies at these corresponding sites are ranged from -72.16 meV to -1.33 meV. However, we would like to note that the hydrogen binding energies at all considered adsorption sites are negative values and this can be understood that hydrogen molecule does not bind with the Zn-ZIF23 host. It is well known that the interaction between hydrogen molecule and the high-surface area materials is the Van der Waals interaction. In order to improve this interaction, the electric dipole moment of host materials must be enhanced. For Zeolitic Imidazolate Framework-23, we modified the ZnN_4 cluster by replacing Zn with either Be or Cd and, again these structures are defined as Be-ZIF23 and Cd-ZIF23, respectively. As clearly shown in Figure 3.11, the organic ligand is the same for

these three structures but only the metal nitride cluster part is different. Hence the hydrogen adsorption energies at the adsorption sites on the organic linker of the Be-, Zn- and Cd- ZIF23 are identical. Owing to this reason, only MN_2 and MN_3 adsorption sites of the M-ZIF23 (M= Be, Zn and Cd) were considered. The hydrogen adsorption energy corresponding to these adsorption sites of the M-ZIF23 are displayed in Figure 3.14.

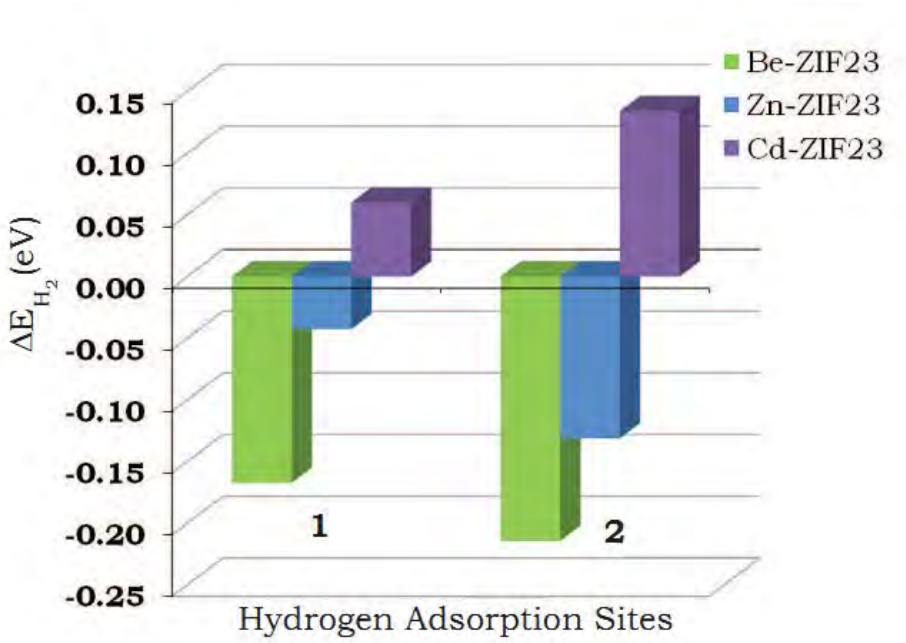

Figure 3.14 Hydrogen binding energies of the M-ZIF23 at MN_3 (site 1 in figure 3.12) and MN_2 (site 2 in figure 3.12) adsorption sites. M stands for Be, Zn and Cd.

According to Figure 3.14, our results revealed that the hydrogen binding energy of the Be-, Zn- and Cd-ZIF23 are -167.43, -42.59 and + 60.05 meV for MN_3 sites (site number 1 in Figure 3.12), respectively. For MN_2 adsorption site (site number 2 in Figure 3.12), we found that the hydrogen binding energies are -214.34, -131.16 and +134.06 meV for Be-, Zn and Cd-ZIF23, respectively. It is clearly seen from these results that Cd-ZIF23 is able to trap hydrogen molecule at both adsorption sites because it gives positive hydrogen adsorption energy, whereas the Be-ZIF23 and Zn-ZIF23 cannot bind hydrogen on their surface. Moreover, trend of hydrogen adsorption energies at these adsorption sites is increased when atomic size of M in metal nitride cluster is gained. It is well known that the interaction between hydrogen and high-surface area materials is the induced dipole-induced dipole interaction or Van der Waals interaction. For Be-, and Zn-ZIF23, the M–N distance (as shown Figure 3.11) is rather short leading to lower electric dipole moment. On the other hand, the electric dipole moment of the Cd-ZIF23 is the largest in comparison to Be- and Zn-ZIF23 due to the longest Cd–N distance.

Based on this result, trend of electric dipole moment of these structures are followed: Cd-ZIF23 > Zn-ZIF23 > Be-ZIF23. This corresponding trend is in excellent agreement with the trend of hydrogen adsorption energy at both MN_2 and MN_3 adsorption sites, namely $\Delta E_{H_2}(\text{Cd-ZIF23}) > \Delta E_{H_2}(\text{Zn-ZIF23}) > \Delta E_{H_2}(\text{Be-ZIF23})$. This leads us to conclude that the increasing in hydrogen binding energy of Cd-ZIF23 comes from the improvement electric dipole moment. Lastly, we believed that this finding can convince both theorist and experimentalist to investigate the practical hydrogen storage medium.

CHAPTER IV

Conclusions

The conclusions are separated into three different parts as discussed in section 4.1-4.3

4.1 Covalent Triazine based Framework -1

Electronic and optical properties of the Covalent Triazine-based Framework-1 were investigated using density functional theory. In the present work, we investigated the optical band gap of four different systems, i.e., CTF-N, CTF-P, CTF-As and CTF-Sb. Our results revealed that the energy gap decreases when the atomic radius of the substituted nonmetals in the triazine ring is increased. In addition, we also varied the concentrations of P and As in CTF-N, which results in partial replacement of N atoms with either P or As atoms. Our results showed that the energy gaps decreased in a non-linearly manner when P and As concentrations were increased in the CTF-N system.

4.2 Covalent Organic Framework-366

Hydrogen adsorption energies of Li decorated Covalent Organic Framework-366 were investigated by means of first-principles calculations. Our results revealed that the center site of the Tetra(p-amino-phenyl) porpyrine and the onN site of the terephthaldehyde chain are the most preferable Li adsorption sites with 2.97 and 2.34 eV of Li binding energies, respectively. In addition, the hydrogen adsorption energies of Li functionalized Covalent Organic Framework-366 range from 0.03 to 0.22 eV for 1-3 H_2 loadings. *Ab initio* molecular dynamics simulations at ambient pressure showed that hydrogen uptakes of Li functionalized Covalent Organic Framework-366 at temperatures of 77, 150 and 298 K are 2.06, 1.58, and 1.05 wt%, respectively.

4.3 Zeolitic Imidazolate Framework-23

The Van der Waals density functional theory is employed to study both electronic and hydrogen adsorption properties of the Be-, Zn- and Cd-ZIF23. According to electronic structure calculations of these systems, our results revealed that only the tetrahedral cluster of metal nitride is altered whereas no change of the 4-Azabenzimidazolate ligand is observed. From the

hydrogen adsorption energy calculations, we found that Be- and Zn-ZIF23 are unable to trap hydrogen molecule on their surface at all considered adsorption sites. In contrast, Cd-ZIF23 is found to be able to bind hydrogen molecule at CdN_2 and CdN_3 sites due to stronger electric dipole moment in comparison to both Be- and Zn-ZIF23.

Acknowledgements

First of all, I would like to thank Associated Professor Vittaya Amornkitbamrung who is my mentor for his constructive and useful suggestions. The Integrated Nanotechnology Research Center (INRC), Nanotec-KKU Center of Excellence on Advanced Nanomaterials for Energy Production and Storage, Thailand Center of Excellence in Physics (ThEP) and the department of physics, faculty of science, Khon Kaen University were acknowledged for providing computer facility. Lastly, this project is financially supported by The Thailand Research Fund (TRF), the Commission on Higher Education (CHE), and Khon Kaen University under contract number MRG5580055.

References

[1] M. A. Green, Solar Cells: Operating Principles, Technology, and System Applications, Prentice-Hall, Inc., 1982.

[2] R. C. Knechli, R. Y. Loo, G. S. Kamath, IEEE Trans. Electron Devices, **31** (1984) 577–588.

[3] F. Kessler, D. Rudmann, Sol. Energy, **77** (2004) 685–695.

[4] A. V. Shah, J. Meier, E. Vallat-Sauvain, N. Wyrsch, U. Kroll, C. Droz, U. Graf, Sol. Energy Mater. Sol. Cells, **78** (2003) 469–491.

[5] K. W. C. Lai, N. Xi, C. K. M. Fung, H. Chen, T.-J. Tarn, Appl. Phys. Lett., **95** (2009) 221107.

[6] N.-M. Park, T.-S. Kim, S.-J. Park, Appl. Phys. Lett., **78** (2001) 2575.

[7] L. Schlapbach, A. Zuttel, Nature, **414** (2001) 353-358.

[8] J. Graetz, Chem. Soc. Rev., **38** (2009) 73-82.

[9] K. L. Lim, H. Kazemian, Z. Yaakob, W. R. W. Daud, Chem. Eng. Technol., **33** (2010) 213-226.

[10] Energy density: http://en.wikipedia.org/wiki/Energy_density

[11] A. Zuttel, Materials Today, **6** (2003) 24-33.

[12] M. G. Nijkamp, J. E. M. J. Raaymakers, A. J. van Dillen, K. P. de Jong, Appl. Phys. a-Mater., **72** (2001) 619-623.

[13] Hydrogen evaporation: http://www.almc.army.mil/alog/issues/MayJun00/MS492.htm.

[14] A. C. Dillon, K. M. Jones, T. A. Bekkedahl, C. H. Kiang, D. S. Bethune, M. J. Heben, Nature, **386** (1997) 377-379.

[15] C. Liu, Y. Y. Fan, M. Liu, H. T. Cong, H. M. Cheng, M. S. Dresselhaus, Science, **286** (1999) 1127-1129.

[16] V. Meregalli, M. Parrinello, Appl. Phys. a-Mater., **72** (2001) 143-146.

[17] R. H. Baughman, A. A. Zakhidov, W. A. de Heer, Science, **297** (2002) 787-792.

[18] N. L. Rosi, J. Eckert, M. Eddaoudi, D. T. Vodak, J. Kim, M. O'Keeffe, O. M. Yaghi, Science, **300** (2003) 1127-1129.

[19] T. Yildirim, M. R. Hartman, Phys. Rev. Lett., **95** (2005) 215504.

[20] L. J. Murray, M. Dinca, J. R. Long, Chem. Soc. Rev., **38** (2009) 1294-1314.

[21] A. Blomqvist, C. M. Araujo, P. Srepusharawoot, R. Ahuja, Proc. Natl. Acad. Sci. USA, **104** (2007) 20173-20176.

[22] J. L. C. Rowsell, A. R. Millward, K. S. Park, O. M. Yaghi, J. Am. Chem. Soc., 126 (2004) 5666-5667.

[23] J. L. C. Rowsell, O. M. Yaghi, Angew. Chem. Int. Edit., **44** (2005) 4670-4679.

[24] J. L. C. Rowsell, O. M. Yaghi, J. Am. Chem. Soc., **128** (2006) 1304-1315.

[25] Q. Sun, P. Jena, Q. Wang, M. Marquez, J. Am. Chem. Soc., **128** (2006) 9741-9745.

[26] D. P. Cao, J. H. Lan, W. C. Wang, B. Smit, Angew. Chem. Int. Edit., **48** (2009) 4730-4733.

[27] P. Srepusharawoot, R. H. Scheicher, C. M. Araujo, A. Blomqvist, U. Pinsook, R. Ahuja, J. Phys. Chem. C, **113** (2009) 8498-8504.

[28] B. Assfour, G. Seifert, Chem. Phys. Lett., **489** (2010) 86-91.

[29] B. Assfour, G. Seifert, Micropor. Mesopor. Mat., **133** (2010) 59-65.

[30] F. Li, J. J. Zhao, B. Johansson, L. X. Sun, Int. J. Hydrogen Energ., **35** (2010) 266-271.

[31] A.. J. Ramirez-Cuesta, P. C. H. Mitchell, D. K. Ross, P. A. Georgiev, P. A. Anderson, H. W. Langmi, D. Book, J. Alloy Compd., **446** (2007) 393-396.

[32] K. P. Prasanth, R. S. Pillai, H. C. Bajaj, R. V. Jasra, H. D. Chung, T. H. Kim, S. D. Song, Int. J. Hydrogen Energ., **33** (2008) 735-745.

[33] M. C. McCarthy, V. Varela-Guerrero, G. V. Barnett, H. K. Jeong, Langmuir, **26** (2010) 14636-14641.

[34] T. Yildirim, H. Wu, W. Zhou, J. Am. Chem. Soc., **129** (2007) 5314.

[35] R. C. Lochan, M. Head-Gordon, Phys. Chem. Chem. Phys., **8** (2006) 1357-1370.

[36] Q. Y. Yang, C. L. Zhong, J. F. Chen, J. Phys. Chem. C, **112** (2008) 1562-1569.

[37] R. Babarao, J.W. Jiang, Langmuir, 24 (2008) 6270-6278.

[38] Z. Y. Guo, H. Wu, G. Srinivas, Y. M. Zhou, S. C. Xiang, Z. X. Chen, Y. T. Yang, W. Zhou, M. O'Keeffe, B. L. Chen, Angew. Chem. Int. Edit., **50** (2011) 3178-3181.

[39] X. M. Lang, S. S. Fan, Y. H. Wang, J .Nat. Gas Chem., **19** (2010) 203-209.

[40] O. M. Yaghi, M. Eddaoudi, J. Kim, N. Rosi, D. Vodak, J. Wachter, M. O'Keeffe, Science, **295** (2002) 469-472.

[41] A. P. Terzyk, S. Furmaniak, P. A. Gauden, P. Kowalczyk, Adsorpt. Sci. Technol., **27** (2009) 281-296.

[42] R. J. Kuppler, D. J. Timmons, Q. R. Fang, J. R. Li, T. A. Makal, M. D. Young, D. Q. Yuan, D. Zhao, W. J. Zhuang, H. C. Zhou, Coordin. Chem. Rev., **253** (2009) 3042-3066.

[43] K. B. Ørnsø, J. M. Garcia-Lastra, K. S. Thygesen, Phys. Chem. Chem. Phys., **15** (2013) 19478-19486.

[44] P. Kuhn, M. Antonietti, A. Thomas, Angew. Chem. Int. Ed. **47** (2008) 3450–3453.

[45] M. J. Bojdys, J. Jeromenok, A. Thomas, M. Antonietti, Adv. Mater. **22** (2010) 2202–2205.

[46] S. Ren, Michael J. Bojdys, R. Dawson, A. Laybourn, Y. Z. Khimyak, D. J. Adams, A. I. Cooper, Adv. Mater. **24** (2012) 2357–2361.

[47] H. Jin, Y. S. Lee, I. Hong, Catal. Today, **120** (2007) 399-406.

[48] F. L. Darkrim, D. Levesque, J. Phys. Chem. B, **104** (2000) 6773-6776.

[49] S. S. Han, H. Furukawa, O. M. Yaghi, W. A. Goddard III. J. Am. Chem. Soc. **130** (2008) 11580-11581.

[50] B. Assfour, G. Seifert . Micropor. Mesopor. Mat. **133** (2010) 59-65.

[51] S. Ma, D. Sun, J. M. Simmons, C. D. Collier, D. Yuan, H.-C. Zhou, J. Am. Chem. Soc. **130** (2007) 1012-1016.

[52] H. Furukawa, O. M. Yaghi, J. Am. Chem. Soc. **131** (2009) 8875-8883 .

[53] C. J. Doonan, D. J. Tranchemontagne, T. G. Glover, J. R. Hunt, O. M. Yaghi., Nat. Chem. **2** (2010) 235-238.

[54] S. Wan, J. Guo, J. Kim, H. Ihee, D. Jiang, Angew. Chem. Int. Ed. **48** (2009) 5439-5442.

[55] S.-Y. Ding, J. Gao, Q. Wang, Y. Zhang, W.-G. Song, C.-Y. Su, W. Wang, J. Am. Chem. Soc., **133** (2011), 19816-19822.

[56] Y. Li, R. T. Yang, AIChE J., **54** (2008) 269–279.

[57] H. Hayashi, A. P. Cote, H. Furukawa, M. O'Keeffe, O. M. Yaghi, Nat. Mater., **6** (2007) 501-506.

[58] R. Babarao, S. Dai, D. E. Jiang, J. Phys. Chem. C, **115** (2011) 8126-8135.

[59] H. Wu, W. Zhou, T. Yildirim, J. Am. Chem. Soc., **129** (2007) 5314-5315.

[60] K. S. Park, Z. Ni, A. P. Cote, J. Y. Choi, R. D. Huang, F. J. Uribe-Romo, H. K. Chae, M. O'Keeffe, O. M. Yaghi, Proc. Natl. Acad. Sci. USA, **103** (2006) 10186-10191.

[61] P. Srepusharawoot, E. Swatsitang, V. Amornkitbamrung, U. Pinsook, R. Ahuja. Int. J. Hydrogen Energ. **38** (2013) 14276-14280.

[62] P. Srepusharawoot, A. Blomqvist, C. M. Araujo. R. H. Scheicher, R. Ahuja. Int. J. Hydrogen Energ. **36** (2011) 555-562.

[63] P. B. Sorokin, H. Lee, L. Y. Antipina, A. K. Singh, B. I. Yakobson, Nano Lett., **11** (2011) 2660-2665.

[64] C. Ataca, E. Akturk, S. Ciraci, Phys. Rev. B, **79** (2009) 041406.

[65] T. Yildirim, S. Ciraci, Phys. Rev. Lett., **94** (2005) 175501.

[66] S. Banerajee, S. Nigam, C. G. S. Pillai, C. Majumder. Int. J. Hydrogen Energ. **37** (2012) 3733-3740.

[67] P. Srepusharawoot, R.H. Scheicher, C.M. Araujo, A. Blomqvist, U. Pinsook, R. Ahuja, J. Phys. Chem. C, **113** (2009) 8498-8504.

[68] P. Hohenberg, W. Kohn, Phys. Rev., **136** (1964) B864-B871.

[69] W. Kohn, L. J. Sham, Phys. Rev., **140** (1965) A1133-A1138.

[70] R. M. Martin. Electronic Structure: Basic Theory and Practical Methods. Cambridge University Press, Cambridge, 2004.

[71] M. W. Finnis J. E. Sinclair, Philos. Mag. A, **50** (1984) 45–55.

[72] J. Tersoff, Phys. Rev. B, **39** (1989) 5566–5568.

[73] P. Zhu, V. Meunier, J. Chem. Phys., **137** (2012) 244703.

[74] J.P. Perdew, K. Burke, M. Ernzerhof, Phys. Rev. Lett., **77** (1996) 3865.

[75] M. Karplus, R.N. Porter, Atoms and Molecules: An Introduction for Students of Physical Chemistry, The Benjamin/Cummings Publishing, 1970.

[76] S. Wan, F. Gándara, A. Asano, H. Furukawa, A. Saeki, S. K. Dey, L. Liao, M. Ambrogio, Y. Y. Botros, X. Duan, S. Seki, J. F. Stoddart, O. M. Yaghi, Chem. Mater. **23** (2011) 4094–4097.

[77] G. Henkelman, A. Arnaldsson, H. Jónsson, Comput. Mater. Sci., **36** (2006) 354–360.

[78] S. Kolmann, S. B. Chan, M. J. T. Jordan, Chem. Phys. Lett., **467** (2008) 126–130.

[79] Q. Sun, P. Jena, Q. Wang, M. Marquez, J. Am. Chem. Soc., **128** (2006) 9741–9745.

[80] Yaghi OM. A joint theory and experimental project in the synthesis and testing of porous COFs for on-board vehicular hydrogen storage. The 2010 progress report for the DOE hydrogen program. p. 595-599, http://www.hydrogen.energy.gov/pdfs/progress10/iv_f_1_yaghi.pdf; 2010.

[81] R. W. Tilford, S. J. Mugavero III, P. J. Pellechia, J. J. Lavigne, Adv. Mater., **20** (2008) 2741–2746.

[82] J. T. Yu, Z. Chen, J. Sun, Z. T. Huang, Q. Y. Zheng, J. Mater. Chem. **22** (2012) 5369–5373.

[83] Z. Guo, H. Wu, G. Srinivas, Y. Zhou, S. Xiang, Z. Chen, Y. Yang, W. Zhou, M. O'Keeffe, B. Chen, Angew. Chem. Int. Ed., **50** (2011) 3178-3181.

[84] J.-H. Guo, H. Zhang, Z.-P. Liu, X.-L. Cheng, J. Phys. Chem. C, **116 (**2012**)** 15908-15917.

[85] R. Banerjee, A. Phan, B. Wang, C. Knobler, H. Furukawa, M. O'Keffee, and O. M. Yaghi, Science, **319** (2008) 939-943.

[86] C. M. Miralda, E. E. Macias, M. Zhu, P. Ratnasamy, M. A. Carreon, ACS Catal., **2** (2012) 180-183.

[87] W. Ma, Q. Jiang, P. Yu, L. Yang, and L. Mao, Anal. Chem. **85** (2013) 7550-7557.

[88] J. Perez-Pellitero, H. Amrouche, F. R. Siperstein, G. Pirngruber, C. Nieto-Draghi, G. Chaplais, A. Simon-Masseron, D. Bazer-Bachi, D. Peralta, and N. Bats, Chem.-Eur. J., **16** (2010) 1560-1571.

[89] A. Phan, C. J. Doonan, F. J. Uribe-Romo, C. B. Knobler, M. O'Keeffe, and O. M. Yaghi, Accounts Chem. Res., **43** (2010) 58 -67.

[90] S. S. Han, S-H. Choi, and W. A. Godard III: J. Phys. Chem. C, **114** (2010) 12039-12047.

[91] W. Zhou, H. Wu, M. R. Hartman, and T. Yildirim: J. Phys. Chem. C, **111** (2007) 16131-16137.

Outputs

Outputs of this project are based on following papers

1. W. Suksaengrat and **P. Srepusharawoot***, Electronic and optical properties of the Covalent Triazine-based Framework-1:First-principles calculations**, Microelectron. Eng.** (2013), 108, 192-194.

2. **P. Srepusharawoot***, E. Swatsitang, V. Amornkitbamrung, U. Pinsook and R. Ahuja, Hydrogen adsorption of Li functionalized Covalent Organic Framework-366: An ab initio study, **Int. J. Hydrogen Energ.** (2013), 38, 14276-14280.

3. S. Wongprakarn, J. Prasongkit and **P. Srepusharawoot***, Hydrogen Adsorption of Be-, Zn-, and Cd- Zeolitic Imidazolate Framework-23: A Comparative Study, (submitted).

*** indicates corresponding author**

APPENDIX

Paper I

W. Suksaengrat and **P. Srepusharawoot**, Electronic and optical properties of the Covalent Triazine-based Framework-1: First-principles calculations**, Microelectron. Eng.** (2013), 108, 192-194.

Microelectronic Engineering 108 (2013) 192–194

Contents lists available at SciVerse ScienceDirect

Microelectronic Engineering

journal homepage: www.elsevier.com/locate/mee

Electronic and optical properties of the Covalent Triazine-based Framework-1: First-principles calculations

W. Suksaengrat [a], P. Srepusharawoot [a,b,c,*]

[a] Department of Physics, Faculty of Science, Khon Kaen University, 40002 Khon Kaen, Thailand
[b] Integrated Nanotechnology Research Center, Khon Kaen University, 40002 Khon Kaen, Thailand
[c] Nanotec-KKU Center of Excellence on Advanced Nanomaterials for Energy Production and Storage, 40002 Khon Kaen, Thailand

ARTICLE INFO

Article history:
Available online 6 February 2013

Keywords:
Covalent Triazine-based Framework-1
Density functional theory
Optical band gap

ABSTRACT

Electronic and optical properties of the Covalent Triazine-based Framework-1 (CTF-N) are determined using density functional theory implemented in the Quantum ESPRESSO program. In the present work, CTF-N was modified by replacing all N atoms with either P, As or Sb atoms, symbolized as CTF-P, CTF-As, and CTF-Sb, respectively. The energy gaps of the corresponding systems were evaluated. Our results revealed that the energy gap trend decreased as atomic radius was increased. These values were 2.02, 0.69, 0.22, and 0 eV for CTF-N, CTF-P, CTF-As and CTF-Sb, respectively. By changing the concentration of either P or As in CTF-N, a non-linear relationship between energy gap and concentrations of P and As was found.

1. Introduction

The energy crisis is an important issue that needs to be solved in the near future. The world's remaining fossil fuel energy resources are rapidly being depleted. Concurrently, annual energy consumption is significantly increasing. This is due to both growth of industries and technologies. Moreover, toxic emissions, especially from automobiles lead to environmental problems. A promising solution to solve these serious issues is the use of renewable energy resources. Use of wind, geothermal, tidal, and hydrogen energy offer some solutions. Solar energy is a promising renewable energy, which is currently receiving much attention. This is because energy obtained from the sun is very abundant. Solar cells or photovoltaic devices are able to generate electrical energy from the sun. The principle of photovoltaic devices is that incident light is used by absorption materials such as crystalline and amorphous Si [1], GaAs [2], copper indium gallium diselenide (CIGS) [3]. Consequently, electrons are excited from their valence bands to their conduction bands. The excited electrons flow through the external load resulting in current generation. In the photon spectra, the maximum photon intensity is in the range from 400 to 600 nm [4]. This wavelength region corresponds to an energy gap (E_g) of about 1.4–3.0 eV. Hence, a suitable E_g for any light absorber should also be in this range in order to maximize solar cell energy conversion efficiency. However, most of materials in nature do not have an E_g in this range. As a result, tuning the energy gap of materials into this desirable range is an essential technique which can be applied to photovoltaic devices and other optically related applications such as sensors [5] and light emitting diodes (LED) [6].

A new material called Covalent Triazine-based Framework-1 (CTF-N) was successfully synthesized [7–9]. CTF-N is thermally stable up to about 600 °C [7]. Its surface area, measured using nitrogen sorption experiments, is 791 m^2/g. The crystal structure of the CTF-N possesses space group P6/mmm. The lattice parameters of this structure are $a = b = 14.574$ Å and $c = 3.4$ Å [7]. The crystal structure of the CTF-N consists of a triazine ring (C_3N_3) covalently bonded with phenyl rings forming a periodic framework. The unit cell of the CTF-N contains 42 atoms consisting of 24 C atoms, 6 N atoms and 12 H atoms. The crystal structure of CTF-N is shown in Fig. 1.

Electronic structure calculations of Zhu and Meunier [10] were done for the CTF-N system using density functional theory (DFT) with a Perdew–Burke–Ernzerhof exchange correlation functional [11]. It was found that CTF-N is a wide band gap semiconductor with a 2.65 eV energy gap. Moreover, they also investigated addition of 2–4 phenyl rings between the triazine rings. Their results showed that the energy gaps decreased when the number of inserted phenyl rings was increased. Kuhn et al. [7] investigated the pore size distribution evaluated using a nonlocal DFT (NLDFT) technique. They found that the pore size of CTF-N was 1.2 nm.

In the present work, the energy gap of the CTF-N was determined by means of density functional theory. We also studied replacement of all N atoms in the triazine ring with either P, As or Sb. These structures are referred to as CTF-P, CTF-As and

* Corresponding author at: Department of Physics, Faculty of Science, Khon Kaen University, 40002 Khon Kaen, Thailand.
E-mail address: spornj@kku.ac.th (P. Srepusharawoot).

0167-9317/$ - see front matter © 2013 Elsevier B.V. All rights reserved.
http://dx.doi.org/10.1016/j.mee.2013.01.037

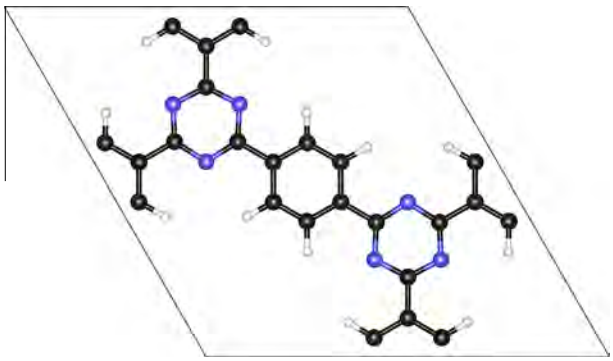

Fig. 1. Crystal structure of the CTF-N. Nitrogen, carbon, and hydrogen atoms are shown as blue, black, and white spheres, respectively. The unit cell of the CTF-N is drawn in black. (For interpretation of the references to color in this figure legend, the reader is referred to the web version of this article.)

CTF-Sb, respectively. The optical band gaps of the CTF-NM (NM = N, P, As and Sb) were determined. Finally, the relationship between the energy gaps and various concentrations of P and As in CTF-N was investigated.

2. Computational details

Electronic and optical properties of all structures under study, i.e., CTF-N, CTF-P, CTF-As and CTF-Sb were computed using the density functional theory implemented in the Quantum ESPRESSO package [12]. For an exchange–correlation functional, the generalized gradient approximation with a Perdew–Wang 91 [13] parameter was chosen. In the current work, the 40 Rydberg plane wave energy cutoff was tested for total energy convergence. Under the Monkhorst–Pack scheme [14], the $2 \times 2 \times 9$ and $4 \times 4 \times 18$ **k**-point samplings of the reciprocal lattice space were used for relaxed and static calculations, respectively. Lastly, the Broyden–Ftetcher–Goldfrab–Shanno (BFGS) algorithm [15–17] was employed for structural optimization.

3. Results and discussion

Structural parameters of CTF-N were determined by optimization with no symmetry constraint. Moreover, other structures were relaxed, e.g., CTF-P, CTF-As and CTF-Sb. P, As and Sb atoms were chosen as replacements for N in CTF-N because they have identical charge states with different atomic sizes, i.e., 0.65, 1.00, 1.15 and 1.45 Å for N, P, As and Sb, respectively [18]. The structural parameters of CTF-NM (NM = N, P, As and Sb) systems are presented in Table 1.

As seen in Table 1, the structural parameters of the CTF-N obtained are in excellent agreement with reported experimental values [7]. For the CTF-P, CTF-As and CTF-Sb systems, the C2–C3 and C3–H distances in Table 1 are unchanged, whereas the NM–C1 distances and the NM–C1–NM bond angles of the CTF-P, CTF-As and CTF-Sb are significantly altered from those of CTF-N. Replacement of N with nonmetal atoms such as P, As and Sb in CTF-N changes only the molecular structure of the NM_3C_3 ring without affecting of the phenyl rings during substitution of N with larger atoms in the CTF-N.

Next, electronic density of states of CTF-NM (NM = N, P, As and Sb) were determined. The corresponding density of states is shown in Fig. 2. It can also be seen that the energy gaps are 2.02, 0.69, 0.22 and 0 eV for CTF-N, CTF-P, CTF-As, and CTF-Sb, respectively. The E_g found are in good agreement to those determined by Zhu and Meunier [10]. The trend of optical band gaps in these considered structures was found to decrease as the covalent radius was increased.

As seen in Fig. 2, the lowest unoccupied states (lowest energy states of the conduction band) lie closer to the Fermi level when we replace N in the CTF-N with larger atoms. This resulted in reducing the optical band gap. To understand the reduction of the optical band gap when larger metals are replaced with N, the partial density of states of the CTF-N states was determined as shown in Fig. 3. According to the partial density of states data, the first peak above the Fermi level primarily comes from the *p* states of N atoms of the triazine ring. This clearly shows that *p* states of nonmetal atoms e.g., P, As and Sb, lead to lower the energy gap seen in Fig. 2. Another reason for the reduction of optical band gaps that replacing N with larger nonmetals in the triazine ring (see Fig. 2) might be from slight distortion of the NM_3C_3 ring. As a consequence, the electronic structures of the CTF-P, CTF-As and CTF-Sb were slightly changed from the intrinsic CTF-N.

As shown in Fig. 2, the band gap can be altered by substituting all N atoms in the triazine ring with either P, As or Sb. Based on this result, changing concentrations of N in the CTF-N with the atoms having equal valence electrons but different atomic sizes can change the optical band gap. In the present work, the concentrations of P and As in the CTF-N were changed by partially replacing N atoms with either P or As. The relationship between the optical band gap and concentrations of P and As in the CTF-N is shown in Fig. 4. Our results reveal that the energy gap exhibited a

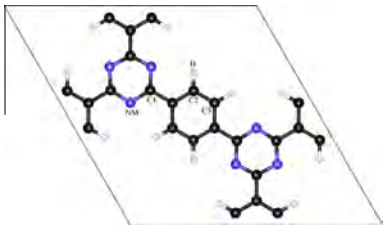

CTF-NM	NM–C1–NM (°)	NM–C1 (Å)	C2–C3 (Å)	C3–H (Å)
CTF-N	124.872	1.345	1.405	1.087
CTF-P	130.391	1.750	1.404	1.089
CTF-As	131.150	1.882	1.405	1.089
CTF-Sb	131.188	2.122	1.415	1.090
CTF-N (exp) [7]	124.385	1.350	1.396	1.085

Table 1: Optimized structural parameters of CTF-NM (NM = N, P, As and Sb). Positions of the NM, C1–C3 and H atoms are presented in the image above the table.

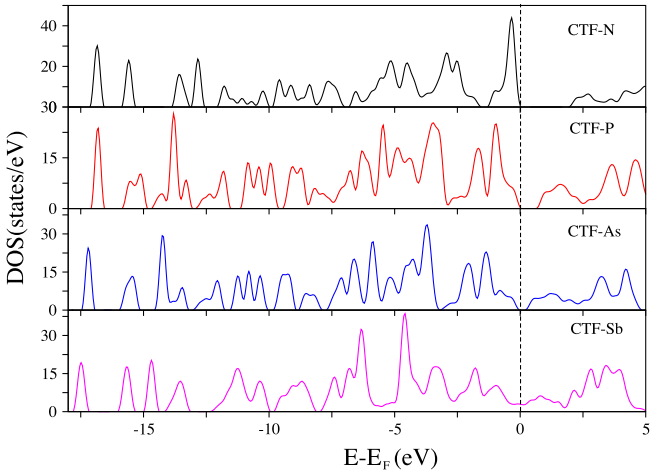

Fig. 2. Electronic density of states of the CTF-N, CTF-P, CTF-As and CTF-Sb. The dotted vertical line represents the Fermi level.

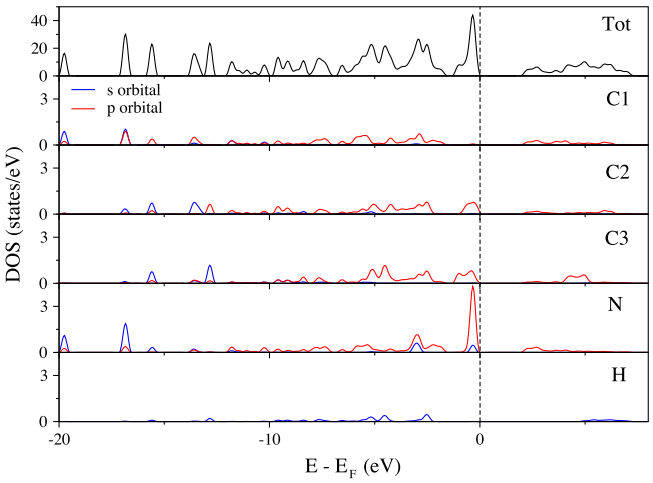

Fig. 3. Total density of states and the partial density of states of N, C1, C2, C3, and H in the CTF-N. The positions of N, C1–C3 and H atoms are presented in Table 1.

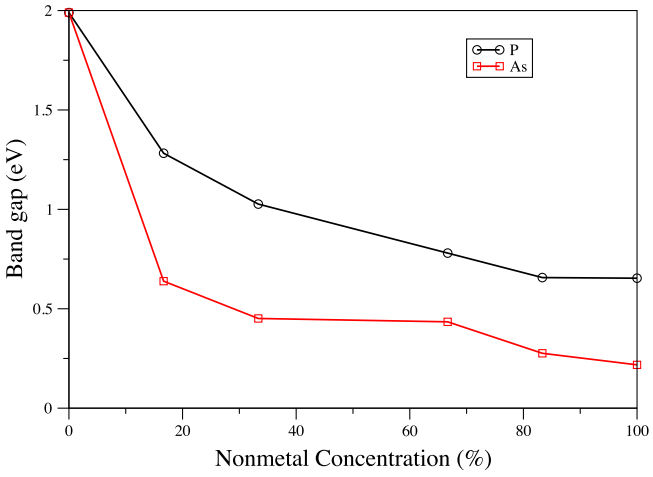

Fig. 4. Relationship between energy gap and various concentrations of P and As in CTF-N.

non-linear drop when P and As concentrations were increased. Moreover, varying Sb concentrations in the CTF-N was considered. Unfortunately, metallic behavior was observed when Sb replaced N in the CTF-N. This is likely caused by the existence of Sb *p* states near the Fermi level causing the optical band gap to vanish. The relationship between the optical band gap and concentrations of both P and As was fitted with a third-order polynomial form as presented below.

$$E_{g,P} = -3.09 \times 10^{-6} c_P^3 + 6.71 \times 10^{-4} c_P^2 - 0.05 c_P + 2.02,$$

$$E_{g,As} = -8.91 \times 10^{-6} c_{As}^3 + 1.67 \times 10^{-3} c_{As}^2 - 0.10 c_{As} + 2.02.$$

where $E_{g,P}$ and $E_{g,As}$ stand for the optical band gap of the CTF-N with various P and As concentrations, respectively. Concentrations of P and As are symbolized as c_P and c_{As}.

Based on these results, it was possible to tune the optical band gap by changing the electronic structure of the materials. In addition, increasing concentrations of P and As in the CTF-N yields non-linear behavior of the optical band gap. Finally, these findings can stimulate both theorists and experimentalists to apply this method to tune the optical band gap of appropriate materials for their use in other optical applications.

4. Conclusions

Electronic and optical properties of the Covalent Triazine-based Framework-1 were investigated using density functional theory implemented in the Quantum ESPRESSO package. In the present work, we investigated the optical band gap of four different systems, i.e., CTF-N, CTF-P, CTF-As and CTF-Sb. Our results revealed that the energy gap decreases when the atomic radius of the substituted nonmetals in the triazine ring is increased. In addition, we also varied the concentrations of P and As in CTF-N, which results in partial replacement of N atoms with either P or As atoms. Our results showed that the energy gaps decreased in a non-linearly manner when P and As concentrations were increased in the CTF-N system.

Acknowledgements

We thank the Thailand Research Fund (TRF) and Commission on Higher Education (CHE) for their financial support under contract number MRG5580055. We express our appreciation to the Integrated Nanotechnology Research Center, Khon Kaen University, the Nanotechnology Center (NANOTEC), NSTDA, Ministry of Science and Technology, Thailand, through its program of Center of Excellence Network for their financial support.

References

[1] M.A. Green, Solar Cells: Operating Principles, Technology, and System Applications, Prentice-Hall, Inc., 1982.
[2] R.C. Knechli, R.Y. Loo, G.S. Kamath, IEEE Trans. Electron Devices 31 (1984) 577–588.
[3] F. Kessler, D. Rudmann, Sol. Energy 77 (2004) 685–695.
[4] A.V. Shah, J. Meier, E. Vallat-Sauvain, N. Wyrsch, U. Kroll, C. Droz, U. Graf, Sol. Energy Mater Sol. Cells 78 (2003) 469–491.
[5] K.W.C. Lai, N. Xi, C.K.M. Fung, H. Chen, T.-J. Tarn, Appl. Phys. Lett. 95 (2009) 221107.
[6] N.-M. Park, T.-S. Kim, S.-J. Park, Appl. Phys. Lett. 78 (2001) 2575.
[7] P. Kuhn, M. Antonietti, A. Thomas, Angew. Chem. Int. Ed. 47 (2008) 3450–3453.
[8] M.J. Bojdys, J. Jeromenok, A. Thomas, M. Antonietti, Adv. Mater. 22 (2010) 2202–2205.
[9] S. Ren, Michael J. Bojdys, R. Dawson, A. Laybourn, Y.Z. Khimyak, D.J. Adams, A.I. Cooper, Adv. Mater. 24 (2012) 2357–2361.
[10] P. Zhu, V. Meunier, J. Chem. Phys. 137 (2012) 244703.
[11] J.P. Perdew, K. Burke, M. Ernzerhof, Phys. Rev. Lett. 77 (1996) 3865.
[12] P. Giannozzi, S. Baroni, N. Bonini, M. Calandra, R. Car, C. Cavazzoni, et al., J. Phys.: Condens. Matter 21 (2009) 395502.
[13] J.P. Perdew, Y. Wang, Phys. Rev. B 45 (1992) 13244–13249.
[14] H.J. Monkhorst, J.D. Pack, Phys. Rev. B 13 (1976) 5188.
[15] R. Fletcher, Practical Methods of Optimization, John Wiley and Sons, 1987.
[16] S.R. Billeter, A.J. Turner, W. Thiel, Phys. Chem. Chem. Phys. 2 (2000) 2177–2186.
[17] S.R. Billeter, A. Curioni, W. Andreoni, Comp. Mater. Sci. 27 (2003) 437–445.
[18] M. Karplus, R.N. Porter, Atoms and Molecules: An Introduction for Students of Physical Chemistry, The Benjamin/Cummings Publishing, 1970.

Paper II

P. Srepusharawoot, E. Swatsitang, V. Amornkitbamrung, U. Pinsook and R. Ahuja, Hydrogen adsorption of Li functionalized Covalent Organic Framework-366: An ab initio study, **Int. J. Hydrogen Energ.** (2013), 38, 14276-14280.

Available online at www.sciencedirect.com

SciVerse ScienceDirect

journal homepage: www.elsevier.com/locate/he

Hydrogen adsorption of Li functionalized Covalent Organic Framework-366: An *ab initio* study

Pornjuk Srepusharawoot [a,b,c,e,*], *Ekaphan Swatsitang* [a,b,c], *Vittaya Amornkitbamrung* [a,b,c,e], *Udomsilp Pinsook* [d,e], *Rajeev Ahuja* [f,g]

[a] *Department of Physics, Faculty of Science, Khon Kaen University, 40002 Khon Kaen, Thailand*
[b] *Integrated Nanotechnology Research Center, Khon Kaen University, 40002 Khon Kaen, Thailand*
[c] *Nanotec-KKU Center of Excellence on Advanced Nanomaterials for Energy Production and Storage, 40002 Khon Kaen, Thailand*
[d] *Department of Physics, Faculty of Science, Chulalongkorn University, 10330 Bangkok, Thailand*
[e] *ThEP, Commission on Higher Education, 328 Si-Ayutthaya Road, 10400 Bangkok, Thailand*
[f] *Condensed Matter Theory Group, Department of Physics and Astronomy, Uppsala University, Box 516, SE-751 20 Uppsala, Sweden*
[g] *Applied Materials Physics, Department of Materials and Engineering, Royal Institute of Technology (KTH), SE-100 44 Stockholm, Sweden*

ARTICLE INFO

Article history:
Received 21 May 2013
Received in revised form
8 August 2013
Accepted 23 August 2013
Available online 21 September 2013

Keywords:
Hydrogen storage
Covalent Organic Framework-366
Hydrogen capacity

ABSTRACT

This work deals with the investigations of hydrogen adsorption energies of the Li functionalized Covalent Organic Framework-366 (COF-366) by using the density functional theory method. Based on total energy calculations, it was found that Li atom is preferentially trapped at the center site of the tetra(p-amino-phenyl) porphyrin and the onN site of a terephthaldehyde chain. Moreover, hydrogen adsorption energies per H_2 for 1–3 H_2 loadings range from 0.03 to 0.22 eV. According to *ab initio* molecular dynamics simulations, our results found that hydrogen capacities of Li functionalized COF-366 at ambient pressure are 2.06, 1.58, and 1.05 wt% for 77, 150 and 298 K, respectively.

1. Introduction

Depletion of fossil fuel based energy resources is a serious global issue. Hydrogen is a promising resource due to its abundance in form of water and its nontoxic combustion products. However, efficiently storing hydrogen is a challenge that needs to be addressed before hydrogen energy can be economically used [1]. The 2015 Department of Energy (DOE) target specifications for hydrogen storage media in onboard applications must be met. Specifically, they must (i) have high hydrogen capacity (9H_2 wt%) (ii) have high hydrogen volumetric uptake (81 gH_2/L) (iii) be inexpensive (iv) operate over the temperature range of −40 to 60 °C (v) have long service life (about 1500 charge/discharge cycles), and, (vi) be environmental friendly [2]. However, no material currently exists that satisfies all of these requirements. At this time, high surface area materials, such as Isoreticular Metal–Organic Frameworks (IRMOFs) [3–5], Covalent Organic Frameworks (COFs)

* *Corresponding author*. Department of Physics, Faculty of Science, Khon Kaen University, 40002 Khon Kaen, Thailand. Tel.: +66 43 203166.
E-mail address: spornj@kku.ac.th (P. Srepusharawoot).
0360-3199/$ – see front matter
http://dx.doi.org/10.1016/j.ijhydene.2013.08.102

[6–9], Covalent Triazine based Frameworks (CTFs) [10] and Zeolitic Imidazolate Frameworks (ZIFs) [11] are promising candidates as hydrogen storage materials. This is due to their great number of hydrogen adsorption sites, tunable pore sizes to trap hydrogen molecules on the host material's surface and ease of hydrogen adsorption/desorption from the host materials. However, hydrogen adsorption energy of these materials is indeed low. As a result, hydrogen is able to bind with the host material under cryogenic conditions. For example, the hydrogen uptake of IRMOF-1 at 77 K and ambient pressure is about 1.32 wt% [12]. Under the same conditions, hydrogen uptake of pristine COF-366 was found to be 1.0 wt% [13]. This corresponds to 0.0684 eV of the isosteric heat of adsorption [13]. With increasing temperature and pressure, the hydrogen capacity of the IRMOF-1 drops to 0.4 wt% at room temperature and 100 bar [14]. To improve hydrogen uptake of these materials, interaction between hydrogen molecules and host material needs to be improved. Currently, many theoretical and experimental studies have shown that decorating metals such as Li [9,15–17], Na [17], K [17], Ca [18], and Ti [19] on the host material's surface is a promising choice to enhance the hydrogen uptake. For instance, at room temperature, the hydrogen capacity of the Li decorated IRMOF-1 at ambient pressure is 2.9 wt% [15]. This is compared to 0.4 wt% for pure IRMOF-1 at 100 bar [14]. Additionally, hydrogen uptake of IRMOF-9 at 298 K and 100 bar was found to be 4.50 wt% and 0.47 wt% with and without Li doping [20]. In this case, the primary reason that hydrogen adsorption energy was enhanced is electrostatic interaction between Li and adsorbed hydrogen molecules. A method of decorating COF-366 with Li atoms is based on an experimental method of producing Li decorated $Cu_3(BTC)_2$ and MIL-101(Cr) [21]. First, lithium naphthalenide was prepared. Then it was mixed with COF-366 and stirred for several hours. The resulting mixture was filtered and rinsed with tetrahydrofuran (THF). Lastly, the mixture was immersed in THF for 1 day in order to remove any weakly adsorbed naphthalenide. It should be noted that the effect of impurities strongly affects hydrogen capacity. This is because the impurities block access to metal cations by hydrogen molecules. This results in lowering the hydrogen adsorption energy. Hence, hydrogen uptake is reduced. Moreover, a reduction method can also be used to insert Li to this material [22]. A post synthetic method is another possible way to functionalize guest molecules, e.g., CH_2Cl_2 [23], $PdCl_2$ [24] to the host. Another method to improve the hydrogen capacity is to make the molecular weight of the host material as low as possible. In other words, host material should be made from light elements such as B, C, N and O. Covalent Organic Frameworks are examples of light-weight materials consisting of only light elements e.g., C, N and H atoms. Recently, a new class of porphyrin based material, covalent organic framework 366 (COF-366), was successfully synthesized [25]. The unit cell of COF-366 possesses a P4/m space group with lattice parameters of $a = b = 25.696$ Å and $c = 12.541$ Å [25]. Its unit cell contains 212 atoms consisting of 120 C atoms, 16 N atoms and 76 H atoms. Moreover, the crystal density and BET surface area of COF-366 are 0.36 g/cm^3 and 735 m^2/g, respectively [25]. The COF-366 crystal structure forms an AA stacking sequence. It has a pore size of 20 Å and an AA interlayer distance of 6.27 Å [25]. Each layer contains tetra(p-amino-phenyl) porphyrin (TAPP) bonded with a terephthaldehyde chain to form the periodic framework as shown in Fig. 1.

In the present work, we theoretically studied the hydrogen adsorption properties of Li decorated COF-366. In addition, the hydrogen capacities of Li functionalized COF-366 at three different temperatures, 77 K, 150 K and 300 K, were evaluated.

2. Computational details

Density functional theory implemented in the Vienna *Ab initio* Simulation Package (VASP) [26] was used to evaluate both Li binding energies and hydrogen adsorption energies. Moreover, the hydrogen capacities at 77, 150, and 298 K were determined by using the Born–Oppenheimer Molecular Dynamics simulations embedded in the VASP code. Using the projector augmented wave (PAW) approach [27], the generalized gradient approximation (GGA) functional with the Perdew-Wang 91 exchange correlation functional [28] was employed. The valence states were 2*s* and 2*p* for both O and C, 1*s* for H, and 1*s* and 2*s* for Li. In the present work, the 450 eV of plane wave cutoff energy was successfully tested and the Γ-point was used for *k*-point sampling in the reciprocal lattice space due to large system size of the COF-366. The conjugate-gradient algorithm was employed for ionic optimization and forces acting on each ion were calculated via the Hellmann–Feynman theorem.

3. Results and discussion

First, geometry optimization with no symmetry constraints was applied to COF-366. We found that our structural

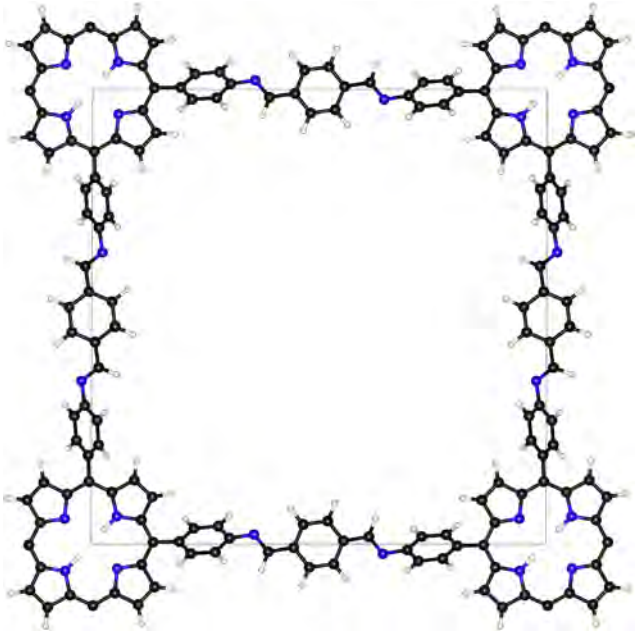

Fig. 1 – The unit cell of COF-366. Blue, black and white spheres are symbolized by N, C and H, respectively. (For interpretation of the references to color in this figure legend, the reader is referred to the web version of this article.)

parameters after optimization differ from experimental data by less than 3%. It was found that $a = 25.493$ Å, $b = 25.488$ Å and $c = 12.144$ Å from our calculation. Experimentally determined values were $a = b = 25.696$ Å and $c = 12.541$ Å [25]. Our computations and experimental results are in excellent agreement.

Then, Li atoms were placed at all possible adsorption sites on COF-366. According to COF-366 crystal geometry, Li atoms can be trapped on both the TAPP and terephthaldehyde chain. On the TAPP, Li atoms can be placed at several locations. These include the center of the pentagon, C–C bridge, onC, onN, N–C bridge of the pentagon ring and at the center of the TAPP. These appear as sites 1–6 in Fig. 2, respectively. Additionally, the positions of Li adsorption sites on the terephthaldehyde chain are the onN, N–C bridge, onC, C–C bridge and hollow sites as shown by sites 7–11 in Fig. 2.

To evaluate the strength of Li interactions to COF-366, Li binding energy (ΔE_{Li}) was determined. It was calculated by:

$$\Delta E_{Li} = E(\mathrm{COF}-366) + E(\mathrm{Li}) - E(\mathrm{COF}-366:\mathrm{Li}).$$

where E(COF-366:Li), E(COF-366) are the total energies of COF-366 with and without Li decorations. The total energy of isolated Li atom is represented as E(Li). The Li binding energies of all considered adsorption sites are given in the Supporting Information. Based on our Li binding energy calculations, we found that the center site (site 6 in Fig. 2) is the most preferable Li adsorption site for Li binding on the TAPP ring. On the terephthaldehyde chain, the onN site (site 7 in Fig. 2) is the most stable adsorption site for Li. The Li binding energies of these two sites were found to be 2.97 eV for the center site and 2.34 eV for the onN site.

Next, various hydrogen loadings ranging from 1 to 3H_2 molecules were placed on Li atoms which were trapped at these adsorption sites. The hydrogen adsorption energy (ΔE_{H_2}) can be calculated by the following:

$$\Delta E_{H_2} = E(\mathrm{COF}-366:\mathrm{Li}) + nE(H_2) - E(\mathrm{COF}-366:\mathrm{Li}+nH_2).$$

where E(COF-366:Li + nH_2) and E(H_2) are the total energies of nH_2 molecules adsorbed on Li decorated COF-366 and the total energy of a free H_2 molecule, respectively.

For a Li atom trapped at the center site, we found that the hydrogen binding energies per H_2 for 1–3 H_2 molecules were 0.13, 0.08 and 0.06 eV, respectively. In addition, the hydrogen adsorption energies per H_2 were 0.22, 0.12 and 0.03 eV when 1–3 H_2 molecules were trapped on Li adsorbed at the onN site. To understand the interaction between Li atoms and adsorbed hydrogen molecules, Bader charge analysis [29] was done for the above cases. Our results showed that 0.9*e* from a Li atom were transferred to COF-366. Hence, the interaction between H_2 molecules and Li atom is governed primarily by charge-quadruple interaction. These results are excellent agreement with previous works [15,30].

Next, several Li atoms were simultaneously placed at the center and onN sites of COF-366. However, it was necessary to determine if Li atoms prefer either trapping on the COF-366's surface (Fig. 3A) or form as a Li cluster at center of the COF-366 pore (Fig. 3B). This leads us to perform total energy calculations for these two cases. In Fig. 3A, we placed 10 Li per unit cell, namely 8 Li at the onN site and 2 Li at the center site. Description of these adsorption sites is shown graphically in Fig. 2. It was found that total energy of Li decorations on the COF-366 surface was lower than that of Li clustered at the center of the COF-366 pore by approximately 1.1 eV/Li atom. In other words, 10 Li atoms are unlikely to form as a cluster at the center of the COF-366 pore. These results are in good agreement with those of both Blomqvist et al. [15] and Sun et al. [31]. To investigate hydrogen uptake of the Li functionalized COF-366 system, a total of 30 H_2 molecules (3 H_2 molecules on each Li atom) were placed on Li decorated COF-366 as an initial configuration. We then preformed *ab initio* molecular dynamics simulations at ambient pressure and temperatures of 77, 150, and 298 K. The 2 fs time step was used in all molecular dynamics calculations. For each temperature, the pair distribution function (PDF) between Li and hydrogen atom was determined. In the present work, the PDFs were averaged over 10 ps at thermodynamic equilibrium for all considered temperatures as shown in Fig. 4. In this Figure, the number of hydrogen atoms adsorbed by Li at each temperature can be obtained by integrating the PDF over the first peak. At 77 K, we found that 3.50 H atoms and 4.01 H atoms are trapped on Li when Li was decorated at the center and onN sites, respectively. By increasing the temperature to 150 K, 2.37 H and 3.14 H can bind with Li atom adsorbed at center and onN sites, respectively. At room temperature, only 1.72 H was able to bind on Li atom trapped at center site. For Li adsorbed at the onN site, it was found that 2.03 H could be trapped on a Li atom. Based on these results, the hydrogen capacities could be calculated. The results showed that hydrogen uptakes at ambient pressure and temperatures of 77, 150, and 298 K were 2.06, 1.58, and 1.05 wt%, respectively. In comparison to experimental data of Yaghi [13], it is clearly shown that the hydrogen capacity of Li doped COF-366 is about 2 times higher than that of pristine COF-366. Hence, it can be seen that enhancement of hydrogen capacity came

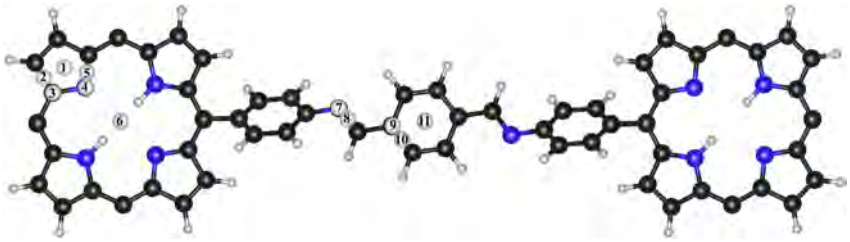

Fig. 2 – Locations of Li adsorption sites in the COF-366. For the adsorption sites on the TAPP, Li can be trapped at center of pentagon ring, C–C bridge, onC, onN, N–C bridge and center site denoted by site numbers 1–6. Numbers 7–11 are the onN, N–C bridge, onC, C–C bridge and hollow sites for the adsorption sites on the terephthaldehyde chain, respectively.

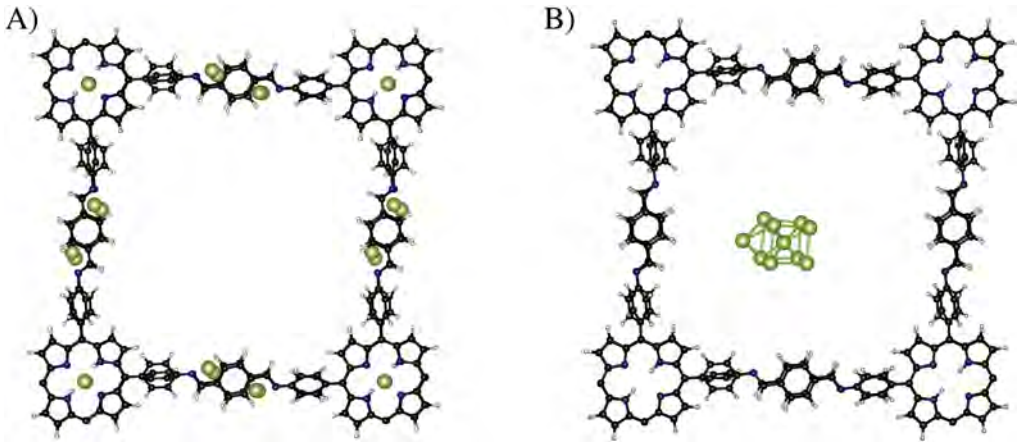

Fig. 3 – Optimized crystal structures of (A) 10 Li atoms trapped on the COF-366 surface, (B) 10 Li atoms formed as a cluster at center of the COF-366 pore. Li, C, N and H are represented as green, black, blue and white spheres, respectively. (For interpretation of the references to color in this figure legend, the reader is referred to the web version of this article.)

from Li doping. Usually, hydrogen uptake by various high surface area materials at 77 K and ambient pressure is less than 2.0 wt%. For example, it is below 1.5 wt% for most of covalent organic frameworks [32,33] and 2.0 wt% for isoreticular metal–organic frameworks [12,34]. However, the hydrogen capacity reported by us is still lower than some other systems, e.g., UTSA-20 [35] and Li functionalized Phthalocyanine Covalent Organic Frameworks [9]. Usually, the hydrogen capacity is gained when the pressure is increased. Hence, it is worth investigating the hydrogen adsorption isotherm. However, our computing resources are limited. Investigation of the hydrogen loading curve as a function of pressure would be extremely time-consuming calculations. This led other independent works to resort to Kinetic Monte Carlo (KMC) [9] and Grand Canonical Monte Carlo (GCMC) [6,36] techniques. These are however beyond the scope of the present work.

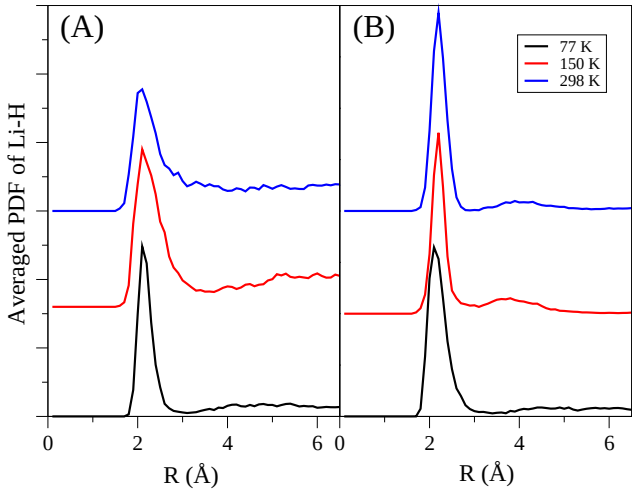

Fig. 4 – The averaged pair distribution functions and distance between Li and hydrogen atoms (R) for the cases of (A) Li trapped at center site and (B) Li adsorbed at the onN.

Based upon the amount of hydrogen adsorbed on Li decorated COF-366, the volumetric hydrogen uptake can also be calculated. We found that they are 8.90, 6.80 and 4.48 g/L for 77, 150 and 298 K, respectively. The volumetric density of Li decorated COF-366 is indeed low owing to rather large unit cell volume.

To make the hydrogen capacity of these materials as high as possible, the host material should be as light as possible. At the same time, it needs to bind a great number of hydrogen molecules. For metal decoration on high surface area materials, Li is a good candidate as a decorating metal for hydrogen storage purposes. This is due to its light weight and rather high interaction energy between hydrogen molecules and host material. Lastly, we propose that functionalization of Li atoms onto a suitable host might be a good strategy to reach the DOE target.

4. Conclusions

Hydrogen adsorption energies of Li decorated Covalent Organic Framework-366 were investigated by means of first-principles calculations. Our results revealed that the center site of the Tetra(p-amino-phenyl) porpyrine and the onN site of the terephthaldehyde chain are the most preferable Li adsorption sites with 2.97 and 2.34 eV of Li binding energies, respectively. In addition, the hydrogen adsorption energies of Li functionalized Covalent Organic Framework-366 range from 0.03 to 0.22 eV for 1–3 H_2 loadings. *Ab initio* molecular dynamics simulations at ambient pressure showed that hydrogen uptakes of Li functionalized Covalent Organic Framework-366 at temperatures of 77, 150 and 298 K are 2.06, 1.58, and 1.05 wt%, respectively.

Acknowledgments

P.S. would like to acknowledge the Thailand Research Fund (TRF) and Commission on Higher Education (CHE) under contract number MRG5580055 for their financial supports. In addition, P.S., E. S. and V. A. also thank the Nanotechnology Center (NANOTEC), NSTDA, Ministry of Science and

Technology, Thailand, through its program of Center of Excellence Network for the research funding. R. A. would like to acknowledge Swedish Research Council, Swedish Energy Agency & Carl Trygress foundation for financial support.

Appendix A. Supplementary data

Supplementary data related to this article can be found at http://dx.doi.org/10.1016/j.ijhydene.2013.08.102.

REFERENCES

[1] Ball M, Wietschel M. The future of hydrogen – opportunities and challenges. Int J Hydrogen Energy 2009;34:615–27.
[2] Satyapal S, Petrovic J, Read C, Thomas G, Ordaz G. The U.S. Department of Energy's national hydrogen storage project: progress towards meeting hydrogen-powered vehicle requirements. Catal Today 2007;120:246–56.
[3] Rosi NL, Eckert J, Eddaoudi M, Vodak DT, Kim J, O'Keeffe M, et al. Hydrogen storage in microporous metal-organic frameworks. Science 2003;300:1127–9.
[4] Srepusharawoot P, Araújo CM, Blomqvist A, Scheicher RH, Ahuja R. A comparative investigation of H_2 adsorption strength in Cd- and Zn-based metal organic framework-5. J Chem Phys 2008;129:164104.
[5] Gomez DA, Sastre G. From microscopic insights of H_2 adsorption to uptake estimations in MOFs. Phys Chem Chem Phys 2011;13:16558–68.
[6] Han SS, Furukawa H, Yaghi OM, Goddard III WA. Covalent organic frameworks as exceptional hydrogen storage materials. J Am Chem Soc 2008;130:11580–1.
[7] Srepusharawoot P, Scheicher RH, Araújo CM, Blomqvist A, Pinsook U, Ahuja R. Ab initio study of molecular hydrogen adsorption in covalent organic framework-1. J Phys Chem C 2009;113:8498–504.
[8] Assfour B, Seifert G. Adsorption of hydrogen in covalent organic frameworks: comparison of simulations and experiments. Micropor Mesopor Mat 2010;133:59–65.
[9] Guo J-H, Zhang H, Liu Z-P, Cheng X-L. Multiscale study of hydrogen adsorption, diffusion, and desorption on Li-doped phthalocyanine covalent organic frameworks. J Phys Chem C 2012;116:15908–17.
[10] Zhang W, Li C, Yuan Y-P, Qiu L-G, Xie A-J, Shen Y-H, et al. Highly energy- and time-efficient synthesis of porous triazine-based framework: microwave-enhanced ionothermal polymerization and hydrogen uptake. J Mater Chem 2010;20:6413–5.
[11] Wu H, Zhou W, Yildirim T. Hydrogen storage in a prototypical zeolitic imidazolate framework-8. J Am Chem Soc 2007;129:5314–5.
[12] Rowsell JLC, Millward AR, Park KS, Yaghi OM. Hydrogen sorption in functionalized metal-organic frameworks. J Am Chem Soc 2004;126:5666–7.
[13] Yaghi OM. A joint theory and experimental project in the synthesis and testing of porous COFs for on-board vehicular hydrogen storage. The 2010 progress report for the DOE hydrogen program. p. 595–9, http://www.hydrogen.energy.gov/pdfs/progress10/iv_f_1_yaghi.pdf; 2010.
[14] Li Y, Yang RT. Hydrogen storage in metal-organic frameworks by bridged hydrogen spillover. J Am Chem Soc 2006;128:8136–7.
[15] Blomqvist A, Araújo CM, Srepusharawoot P, Ahuja R. Li-decorated metal-organic framework 5: a route to achieving a suitable hydrogen storage medium. Proc Nat Acad Sci U S A 2007;104:20173–6.
[16] Konstas K, Taylor JW, Thornton AW, Doherty CM, Lim WX, Bastow TJ, et al. Lithiated porous aromatic frameworks with exceptional gas storage capacity. Angew Chem Int Ed 2012;51:6639–42.
[17] Srepusharawoot P, Blomqvist A, Araújo CM, Scheicher RH, Ahuja R. Hydrogen binding in alkali-decorated iso-reticular metal organic framework-16 based on Zn, Mg, and Ca. Int J Hydrogen Energy 2011;36:555–62.
[18] Ataca C, Aktürk E, Ciraci S. Hydrogen storage of calcium atoms adsorbed on graphene: first-principles plane wave calculations. Phys Rev B 2009;79:041406.
[19] Yildirim T, Ciraci S. Titanium-decorated carbon nanotubes as a potential high-capacity hydrogen storage medium. Phys Rev Lett 2005;94:175501.
[20] Meng Z, Lu R, Rao D, Kan E, Xiao C, Deng K. Cartenated metal-organic frameworks: promising hydrogen purification materials and high hydrogen storage medium with further lithium doping. Int J Hydrogen Energy 2013;38:9811–8.
[21] Xiang Z, Hu Z, Yang W, Cao D. Lithium doping on metal-organic frameworks for enhancing H_2 storage. Int J Hydrogen Energy 2012;37:946–50.
[22] Mulfort KL, Hupp JT. Chemical reduction of metal-organic framework materials as a method to enhance gas uptake and binding. J Am Chem Soc 2007;129:9604–5.
[23] Wang Z, Cohen SM. Postsynthetic covalent modification of a neutral metal-organic framework. J Am Chem Soc 2007;129:12368–9.
[24] Cohen SM. Postsynthetic methods for the functionalization of metal-organic frameworks. Chem Rev 2012;112:970–1000.
[25] Wan S, Gándara F, Asano A, Furukawa H, Saeki A, Dey SK, et al. Covalent organic frameworks with high charge carrier mobility. Chem Mater 2011;23:4094–7.
[26] Kresse G, Furthmüller J. Efficiency of ab-initio total energy calculations for metals and semiconductors using a plane-wave basis set. Comput Mater Sci 1996;6:15–50.
[27] Blöchl PE. Projector augmented-wave method. Phys Rev B 1994;50:17953–79.
[28] Perdew JP, Wang Y. Accurate and simple analytic representation of the electron-gas correlation energy. Phys Rev B 1992;45:13244–9.
[29] Henkelman G, Arnaldsson A, Jónsson H. A fast and robust algorithm for Bader decomposition of charge density. Comput Mater Sci 2006;36:354–60.
[30] Kolmann SJ, Chan B, Jordan MJT. Modelling the interaction of molecular hydrogen with lithium-doped hydrogen storage materials. Chem Phys Lett 2008;467:126–30.
[31] Sun Q, Jena P, Wang Q, Marquez M. First-principles study of hydrogen storage on $Li_{12}C_{60}$. J Am Chem Soc 2006;128:9741–5.
[32] Tilford RW, Mugavero III SJ, Pellechia PJ, Lavigne JJ. Tailoring microporosity in covalent organic frameworks. Adv Mater 2008;20:2741–6.
[33] Yu J-T, Chen Z, Sun J, Huang Z-T, Zheng Q-Y. Cyclotricatechylene based porous crystalline material: synthesis and applications in gas storage. J Mater Chem 2012;22:5369–73.
[34] Rowsell JLC, Yaghi OM. Effects of functionalization, catenation, and variation of the metal oxide and organic linking units on the low-pressure hydrogen adsorption properties of metal-organic frameworks. J Am Chem Soc 2006;128:1304–15.
[35] Guo Z, Wu H, Srinivas G, Zhou Y, Xiang S, Chen Z, et al. A metal-organic framework with optimized open metal sites and pore spaces for high methane storage at room temperature. Angew Chem Int Ed 2011;50:3178–81.
[36] Guo J-H, Zhang H, Gong M, Cheng X-L. Ca^{2+}- and Mg^{2+}-doped covalent organic frameworks exhibiting high hydrogen and acetylene storage. Struct Chem 2013;24:691–703.

Supporting Information

Pornjuk Srepusharawoot[a,b,c,e], Ekaphan Swatsitang[a,b,c], Vittaya Amornkitbamrung[a,b,c,e] , Udomsilp Pinsook[d,e], Rajeev Ahuja[f,g]

[a]Department of Physics, Faculty of Science, Khon Kaen University, 40002, Khon Kaen, Thailand.
[b]Integrated Nanotechnology Research center, Khon Kaen University, 40002, Khon Kaen, Thailand.
[c]Nanotec-KKU Center of Excellence on Advanced Nanomaterials for Energy Production and Storage, 40002, Khon Kaen, Thailand.
[d]Department of Physics, Faculty of Science, Chulalongkorn University, 10330, Bangkok, Thailand.
[e]ThEP, Commission on Higher Education, 328 Si-Ayutthaya road, 10400, Bangkok, Thailand.
[f]Condensed Matter Theory Group, Department of Physics and Astronomy, Uppsala University, Box 516, SE-751 20 Uppsala, Sweden
[g]Applied Materials Physics, Department of Materials and Engineering, Royal Institute of Technology (KTH), SE-100 44 Stockholm, Sweden

S1. Li binding energies of the COF-366

Figure S1 shows the results of Li binding energies at all considered adsorption sites graphically displayed in Figure 2 in the manuscript. It was clearly seen that Li atom preferably traps at the center site (site 6) of the TAPP ring. For the terephthaldehyde chain, the onN site (site 7) was found to be the most stable adsorption site of Li.

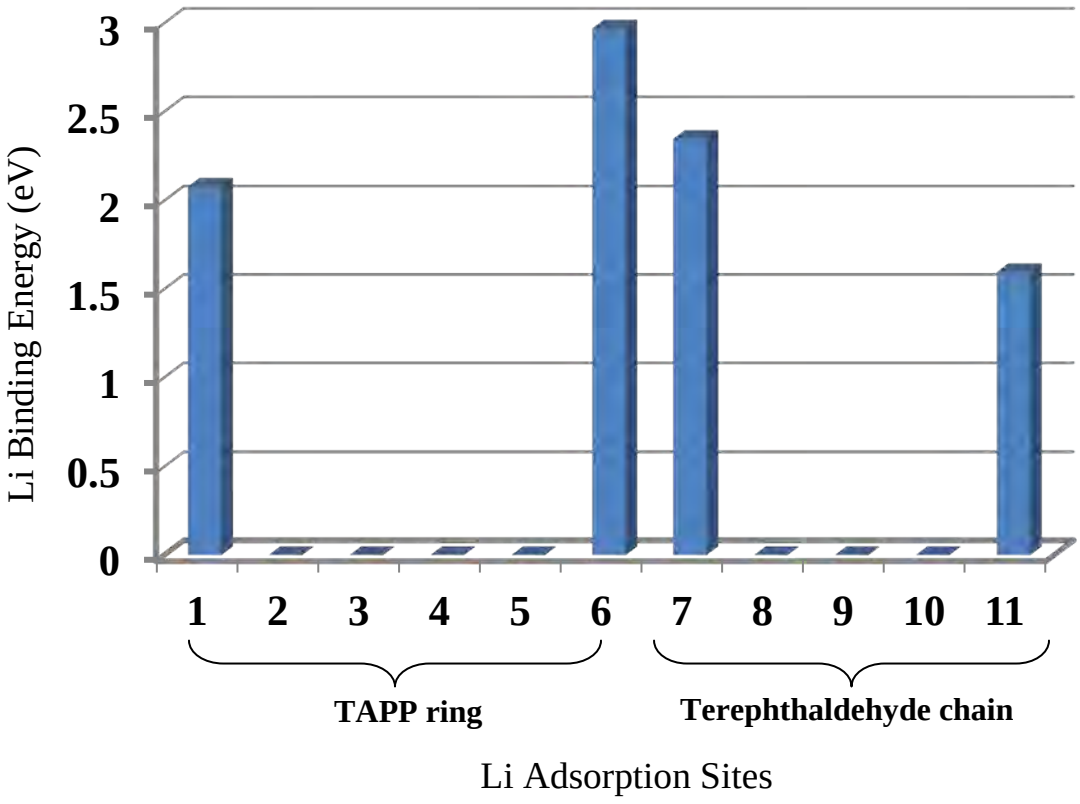

Figure S1. Li adsorption energies at various adsorption sites. The position of sites 1-7 are graphically shown in Figure 2 of the manuscript. For unstable adsorption sites, Li binding energy is set to be zero.

Paper III

S. Wongprakarn, J. Prasongkit and **P. Srepusharawoot**, Hydrogen Adsorption of Be-, Zn-, and Cd- Zeolitic Imidazolate Framework-23: A Comparative Study, (submitted).

Hydrogen Adsorption of Be-, Zn-, and Cd- Zeolitic Imidazolate Framework-23: A Comparative Study

S. Wongprakarn[1], J. Prasongkit[2] and P. Srepusharawoot[3,4,5] *

[1] *Materials Science and Nanotechnology program, Faculty of Science, Khon Kaen University, 40002 Khon Kaen, Thailand.*

[2] *Division of Science, Faculty of Liberal Arts and Science, Nakhon Phanom University, 48000 Nakhon Phanom, Thailand.*

[3] *Department of Physics, Faculty of Science, Khon Kaen University, 40002 Khon Kaen, Thailand.*

[4] *Integrated Nanotechnology Research Center, Khon Kaen University, 40002 Khon Kaen, Thailand.*

[5] *Nanotec-KKU Center of Excellence on Advanced Nanomaterials for Energy Production and Storage, 40002 Khon Kaen, Thailand.*

Hydrogen adsorption energies of Be-, Zn-, and Cd- Zeolitic Imidazolate Framework-23 were investigated by using Van der Waals density functional theory implemented in Quantum ESPRESSO program. According to the structural parameters of these systems, we found that the imidazole ligand is unchanged and only the tetrahedrally metal nitride cluster is varied. Moreover, our results revealed that the Cd-Zeolitic Imidazolate Framework-23 has the highest electric dipole moment followed by Zn- and Be- Zeolitic Imidazolate Framework-23. Based on hydrogen adsorption energy calculations, we found that hydrogen molecule can not bind with both Be- and Zn- Zeolitic Imidazolate Framework-23 at all considered adsorption sites, whereas hydrogen molecule can trap on the Cd-Zeolitic Imidazolate Framework-23 with the hydrogen binding energies ranged from 60 to 130 meV. This result suggested that replacing Zn in the metal nitride cluster with larger metal size can enhance the hydrogen adsorption energy of Zeolitic Imidazolate Framework-23.

1. Introduction

It has long been known that energy crisis and global warming issues are expected to be very serious issues in the near future. Hydrogen energy is a solution of these problems due to its abundance and clean product. However, it is very difficult to store hydrogen gas into the hydrogen storage medium because its density is indeed low, namely 0.088 kg/m^3.[1)] As a result, size of storage medium is very big. Therefore, one challenge task of many researchers is to investigate the suitable hydrogen storage medium for practical applications. Based on the 2015 DOE requirements,[2)] the hydrogen storage medium must (i) have high hydrogen capacity (9 H_2 wt %) and high hydrogen volu-

*E-mail address: spornj@kku.ac.th

metric uptake (81 gH_2/L) (ii) be cheap (iii) operate over the temperature range of -40 to 60 ^oC (iv) have long service life (about 1500 charge/discharge cycles), and (v) be environmental friendly. Currently, storing hydrogen in high-surface area materials such as Metal Organic Frameworks (MOFs),[3–6] Covalent Organic frameworks (COFs),[7–10] Carbonaceous materials,[11–13] Zeolite,[14,15] Zeolitic imidazolate Frameworks (ZIFs)[16,17] have been shown to be promising hydrogen storage materials because they contain numerous number of hydrogen adsorption sites, easy to trap/release hydrogen and tunable pore size. Besides the surface area and pore size of the host material, another important parameter related to the hydrogen capacity is the hydrogen adsorption energy. For practical application, the ideal hydrogen adsorption energy should be about 40 kJ/mol.[18] Although, for most of high-surface area materials, the hydrogen adsorption energy is very low because the interaction between adsorbed hydrogen molecules and the materials is governed by weak dispersive interaction. Currently there are several approaches[19–22] to improve the hydrogen adsorption energy of the high-surface area materials. One successful route shown by Srepusharawoot *et al.*[23] is to open the metal oxide cluster of the MOF-5 by replacing Zn with Cd. They found that the hydrogen adsorption energy is improved for 15 % for the adsorption sites near metal oxide cluster.

Zeolitic imidazolate frameworks (ZIFs) are new classes of high-surface area materials, successfully synthesized by Yaghi 's research group.[24,25] As shown by Banerjee *et al.*,[25] both pore size and surface area of these materials can be tuned by adjustment the metal nitride (MN_4) unit (M=Zn, Co, Cu) and imidazole ligands. Consequently, the ZIFs can be used in various applications such as catalyst,[26] biosensor,[27] gas storage media e.g. N_2,[28] CO_2[28,29] and CH_4.[28] Based on both theoretical and experimental studies,[16,30] ZIFs show great promise of hydrogen storage materials. According to neutron diffraction experiments at 30 K and ambient pressure,[16] ZIF-8 can trap 28 hydrogen molecules corresponding to 4.2 H_2 wt%. By increasing the temperature to 77 K and 1 bar of pressure, the hydrogen capacity is dramatically decreased to 1.3 wt%.[31] Based on the grand canonical Monte Carlo simulations, ZIF-11 can uptake hydrogen about 3.96 wt% at 77 K and 100 bar. When the pressure is reduced to 1 bar, the hydrogen uptake is slightly dropped to 2.39 wt%.[32] For Zeolitic imidazolate framework-23 (ZIF-23), there is no report in the literature related to the hydrogen adsorption. Thus this motivates us to investigate the hydrogen adsorption properties of this system.

For ZIF-23 or Zn-ZIF23 system, it consists of tetrahedral cluster of ZnN_4 covalently bonded to the 4-Azabenzimidazolate as an organic linker. Its unit cell contains 108

atoms consisting of 4 Zn atoms, 24 N atoms, 48 C atoms and 32 H atoms. The crystal structure of the ZIF-23 is an orthorhombic crystal system with space group P212121. The lattice constants are $a = 9.5477$ Å $b = 10.1461$ Å and $c = 12.4459$ Å. Its crystal density is 1.662 g/cm^3.[24] In the present work, we investigated the structural parameters and the hydrogen adsorption energies of Be-, Zn- and Cd- based ZIF23 structures, referred to in the following as Be-ZIF23, Zn-ZIF23 and Cd-ZIF23. The crystal structure of the M-ZIF23 (M= Be, Zn, and Cd) are shown in Figure 1.

2. Computational Details

Electronic and hydrogen adsorption properties of the M-ZIF23 (M= Be, Zn and Cd) were investigated by using the Van der Waals density functional theory (vdw-DF)[33,34] implemented in Quantum ESPRESSO code.[35] The 60 Rydberg of plane wave energy cutoff was tested for total energy convergence and the 3×3×1 **k**-point samplings with the Monkhorst-Pack scheme[36] was chosen in the present work. Finally, the Broyden-Fletcher-Goldfrab-Shanno (BFGS) algorithm[37,38] was employed for structural optimization.

3. Results and Discussion

3.1 Structural Parameters of the Be-, Zn- and Cd-ZIF23

First, the Be-, Zn- and Cd-ZIF23 were fully relaxed by discarding the symmetry constraint. The structural parameters after optimization are listed in Figure 2.

According to Figure 2, it is clearly seen that the structural parameters of the Zn-ZIF23 are in excellent agreement with the experimental data.[24] Hence, our calculation results are rather accurate. By considering ionic radius of Be, Zn and Cd, the atomic size of Cd is the largest followed by Zn and Be. The ionic radii of Be, Zn and Cd are 0.59, 0.88 and 1.09 Å respectively. As shown in Figure 2, our results revealed that the N–C1, C2–C3 and C3–C4 distances are unchanged, whereas M–N distances of these structures are increased when atomic size of M atoms is gained. This leads to the fact that there is no any effect to the imidazole ring due to the different in size of M atoms at the tetrahedral cluster. Moreover, we found that the M–N distances are increased resulting in improvement of the electric dipole moment when size of M in metal nitride cluster is gained. Based on these results, the electric dipole moment of Cd-ZIF23 is the highest followed by Zn-ZIF23 and Be-ZIF23.

3.2 Hydrogen Adsorption of the Be-, Zn- and Cd-ZIF23

In this section, we place single hydrogen molecule at various adsorption sites of M-ZIF23 structures and then investigated the hydrogen adsorption energies of these structures. We firstly considered the adsorption sites of Zn-ZIF23. Based on the crystal geometry of the Zn-ZIF23, we can divide the adsorption sites into two different parts, namely the adsorption sites near tetrahedral ZnN_4 cluster and on the 4-Azabenzimidazolate ligand. The adsorption sites near the ZnN_4 cluster consists of two locations, namely ZnN_3 and ZnN_2 as labeled by sites number 1 and 2 in Figure 3. Moreover, there are 10 different hydrogen adsorption sites on the organic ligand considered in the present work. For the pentagon ring of carbon in the organic ligand, hydrogen molecule can trap at center of the pentagon rings (number 3), top of N (number 4), top of C (number 5), C–C bridge (number 6), top of C connected to hexagon ring (number 7). In addition, there are 5 different adsorption sites on the hexagon ring of the organic ligand represented by the sites number 8–12 in Figure 3.

To investigate the interaction between hydrogen molecule and the Zn-ZIF23, the hydrogen binding energy at a particular adsorption site is determined. It can be given by

$$\Delta E_{H_2} = E(\text{Zn-ZIF23}) + E(\text{H}_2) - E(\text{Zn-ZIF23:H}_2),$$

where E(Zn-ZIF23) and $E(\text{H}_2)$ stand for total energy of isolated Zn-ZIF23 and H_2 molecule, respectively. E(Zn-ZIF23:H_2) is total energy of single hydrogen molecule adsorbed on the Zn-ZIF23 structure. According to above equation, the positive ΔE_{H_2} implies that hydrogen molecule can adsorb on the Zn-ZIF23 host. In contrast, the hydrogen molecule is unable to trap on the Zn-ZIF23 host leading to the negative value of ΔE_{H_2}. The calculated hydrogen adsorption energies of the Zn-ZIF23 at 12 different sites are displayed in Figure 4.

As clearly seen in Figure 4, the hydrogen binding energies at ZnN_2 and ZnN_3 adsorption sites are -131.16 and -42.59 meV, respectively. By considering the adsorption sites on the 4-Azabenzimidazolate ligand, the hydrogen adsorption energies at these corresponding sites are ranged from -72.16 meV to -1.33 meV. However, we would like to note that the hydrogen binding energies at all considered adsorption sites are negative values and this can be understood that hydrogen molecule does not bind with the Zn-ZIF23 host. It is well known that the interaction between hydrogen molecule and the high-surface area materials is the Van der Waals interaction. In order to improve

this interaction, the electric dipole moment of host materials must be enhanced. For Zeolitic Imidazolate Framework-23, we modified the ZnN_4 cluster by replacing Zn with either Be or Cd and, again these structures are defined as Be-ZIF23 and Cd-ZIF23, respectively. As clearly shown in Figure 2, the organic ligand is the same for these three structures but only the metal nitride cluster part is different. Hence the hydrogen adsorption energies at the adsorption sites on the organic linker of the Be-, Zn- and Cd- ZIF23 are identical. Owing to this reason, only MN_2 and MN_3 adsorption sites of the M-ZIF23 (M= Be, Zn and Cd) were considered. The hydrogen adsorption energy corresponding to these adsorption sites of the M-ZIF23 are displayed in Figure 5.

According to Figure 5, our results revealed that the hydrogen binding energy of the Be-, Zn- and Cd-ZIF23 are -167.43, -42.59 and + 60.05 meV for MN_3 sites (site number 1 in Figure 3), respectively. For MN_2 adsorption site (site number 2 in Figure 3), we found that the hydrogen binding energies are -214.34, -131.16 and +134.06 meV for Be-, Zn- and Cd-ZIF23, respectively. It is clearly seen from these results that Cd-ZIF23 is able to trap hydrogen molecule at both adsorption sites because it gives positive hydrogen adsorption energy, whereas the Be-ZIF23 and Zn-ZIF23 can not bind hydrogen on their surface. Moreover, trend of hydrogen adsorption energies at these adsorption sites is increased when atomic size of M in metal nitride cluster is gained. It is well known that the interaction between hydrogen and high-surface area materials is the induced dipole-induced dipole interaction or Van der Waals interaction. For Be- and Zn-ZIF23. the M–N distance as shown Figure 2 is rather short leading to lower electric dipole moment. On the other hand, the electric dipole moment of the Cd-ZIF23 is the largest in comparison to Be- and Zn-ZIF23 due to the longest Cd–N distance. Based on this result, trend of electric dipole moment of these structures are followed: Cd-ZIF23 > Zn-ZIF23 > Be-ZIF23. This corresponding trend is in excellent agreement with the trend of hydrogen adsorption energy at both MN_2 and MN_3 adsorption sites, namely ΔE_{H_2}(Cd-ZIF23) > ΔE_{H_2}(Zn-ZIF23) > ΔE_{H_2}(Be-ZIF23). This leads us to conclude that the increasing in hydrogen binding energy of Cd-ZIF23 comes from the improvement electric dipole moment. Lastly, we believed that this finding can convince both theorist and experimentalist to investigate the practical hydrogen storage medium.

4. Conclusions

The Van der Waals density functional theory is employed to study both electronic and hydrogen adsorption properties of the Be-, Zn- and Cd-ZIF23. According to electronic

structure calculations of these systems, our results revealed that only the tetrahedral cluster of metal nitride is altered whereas no change of the 4-Azabenzimidazolate ligand is observed. From the hydrogen adsorption energy calculations, we found that Be- and Zn-ZIF23 are unable to trap hydrogen molecule on their surface at all considered adsorption sites. In contrast, Cd-ZIF23 is found to be able to bind hydrogen molecule at CdN_2 and CdN_3 sites due to stronger electric dipole moment in comparison to both Be- and Zn-ZIF23.

Acknowledgments

We express our appreciation to the Integrated Nanotechnology Research Center, Khon Kaen University and the Nanotechnology Center (NANOTEC), NSTDA, Ministry of Science and Technology, Thailand, through its program of Center of Excellence Network for their financial supports. P.S. would like to thank the Thailand Research Fund (TRF) and Commission on Higher Education (CHE) under contract number MRG5580055 for their research grant.

References

1) C. Kittel: *Introduction to Solid State Physics*(Wiley, New Jersey, 2005) 8th ed., p. 21.
2) S. Satyapal, J. Petrovic, C. Read, G. Thomas, and G. Ordaz: Catal. Today **120** (2007) 246.
3) N. L. Rosi, J. Eckert, M. Eddaoudi, D. T. Vodak, J. Kim, M. O'Keeffe, and O. M. Yaghi: Science **300** (2003) 1127.
4) P. Srepusharawoot, A. Blomqvist, C. M. Araújo , R. H. Scheicher, and R. Ahuja: Int. J. Hydrogen Energ. **36** (2011) 555.
5) W-X. Lim, A. W. Thornton, A. J. Hill, B. J. Cox, J. M. Hill, and M. R. Hill: Langmuir **29** (2013) 8524.
6) H. J. Park and M. P. Suh: Chem. Commun. **48** (2012) 3400.
7) P. Srepusharawoot, R. H. Scheicher , C. M. Araújo, A. Blomqvist , U. Pinsook, and R. Ahuja: J. Phys. Chem. C **113** (2009) 8498.
8) P. Srepusharawoot, E. Swatsitang, V. Amornkitbamrung, U. Pinsook, and R. Ahuja: Int. J. Hydrogen Energ. **38** (2013) 14276.
9) B. Assfour, and G. Seifert: Micropor. Mesopor. Mat. **133** (2010) 59.
10) K. T. Jackson, T. E. Reich, and H. M. El-Kaderi: Chem. Commun. **48** (2012) 8823.
11) H-L. Park, D. S. Yoo, and Y-C. Chung: Jpn. J. Appl. Phys. **50** (2011) 06GJ02.
12) T. Roman, W. A. Dino, H. Nakanishi, H. Kasai, T. Sugimoto, and K. Tange: Jpn. J. Appl. Phys. **45** (2006) 1765.
13) L. Wang, and R. T. Yang: Carbon **50** (2012) 3134.
14) N. P. Stadie, J. J. Vajo, R. W. Cumberland, A. A. Wilson, C. C. Ahn, and B. Fultz: Langmuir **28** (2012) 10057.
15) J. Dong, X. Wang, H. Xu, Q. Zhao, and J. Li: Int. J. Hydrogen Energ. **32** (2007) 4998.
16) H. Wu, W. Zhou, and T. Yildirim: J. Am. Chem. Soc. **129** (2007) 5314.
17) M. Zhou, Q. Wang, L. Zhang, Y-C. Liu, and Y. Kang: J. Phys.Chem. B **113** (2009) 11049.
18) V. Bérubé, G. Radtke, M. Dresselhaus, and G. Chen: Int. J. Energy Res. **31** (2007) 637.
19) Y. Li, and R. T. Yang: J. Am. Chem. Soc. **128** (2006) 8136.
20) A. Blomqvist, C. M. Araújo, P. Srepusharawoot, and R. Ahuja: P. Natl. Acad. Sci.

U.S.A. **104** (2007) 20173.

21) J. L. C. Rowsell, and O. M. Yaghi: J. Am. Chem. Soc. **128** (2006) 1304.

22) B. Chen, N. W. Ockwig, A. R. Millward, D. S. Contreras, and O. M. Yaghi: Angew. Chem. Int. Edit. **44** (2005) 4745.

23) P. Srepusharawoot, C. M. Araújo , A. Blomqvist, R. H. Scheicher, and R. Ahuja: J. Chem. Phys. **129** (2008) 164104.

24) H. Hayashi, A. P. Côte, H. Furukawa, M. O'Keffee, and O. M. Yaghi: Nat. Mater. **6** (2007) 501.

25) R. Banerjee, A. Phan, B. Wang, C. Knobler, H. Furukawa, M. O'Keeffe, and O. M. Yaghi: Science **319** (2008) 939.

26) C. M. Miralda, E. E. Macias, M. Zhu, P. Ratnasamy,and M. A. Carreon: ACS Catal. **2** (2012) 180.

27) W. Ma, Q. Jiang, P. Yu, L. Yang, and L. Mao: Anal. Chem. **85** (2013) 7550.

28) J. Pérez-Pellitero, H. Amrouche, F. R. Siperstein, G. Pirngruber, C. Nieto-Draghi,G. Chaplais, A. Simon-Masseron, D. Bazer-Bachi, D. Peralta, and N. Bats: Chem.-Eur. J. **16** (2010) 1560.

29) A. Phan, C. J. Doonan, F. J. Uribe-Romo, C. B. Knobler, M. O'Keeffe, and O. M. Yaghi: Accounts Chem. Res. **43** (2010) 58.

30) S. S. Han, S-H. Choi, and W. A. Godard III: J. Phys. Chem. C **115** (2011) 3507.

31) W. Zhou, H. Wu, M. R. Hartman, and T. Yildirim: J. Phys. Chem. C **111** (2007) 16131.

32) S. S. Han, S-H. Choi, and W. A. Godard III: J. Phys. Chem. C **114** (2010) 12039.

33) M. Dion, H. Rydberg, E. Schröder, D. C. Langreth, and B. I. Lundqvist: Phys. Rev. Lett. **92** (2004) 246401.

34) T. Thonhauser, V. R. Cooper, S. Li, A. Puzder, P. Hyldgaard, and D. C. Langreth: Phys. Rev. B **76** (2007) 125112.

35) P. Giannozzi, S. Baroni, N. Bonini, M. Calandra, *et al.* J. Phys.-Condens. Mat. **21** (2009) 395502.

36) H. J. Monkhorst, and J. D. Pack: Phys. Rev. B **13** (1976) 5188.

37) S. R. Billeter, A. J. Turner, and W. Thiel: Phys. Chem. Chem. Phys. **2** (2000) 2177.

38) S. R. Billeter, A. Curioni, and W. Andreoni: Comp. Mater. Sci. **27** (2003) 437.

Figure captions

Fig.1 Crystal structure of the M-ZIF23 (M = Be, Zn and Cd). M, N, C and H atoms are denoted by blue, green, black and white spheres, respectively. The solid line represents the unit cell of the M-ZIF23.

Fig.2 Structural parameters of M-ZIF23 (M = Be, Zn and Cd) after performing structural optimization. Positions of M, N, C1–C4 are presented at picture above.

Fig. 3 Hydrogen adsorption sites of the M-ZIF23 (M = Be, Zn and Cd). Blue, green, black and white spheres are represented as M, N, C and H, respectively.

Fig. 4 Hydrogen adsorption energies of the Zn-ZIF23 at 12 different adsorption sites. The numbers of adsorption sites shown here are referred to the number of adsorption sites in Figure 3. We would like to note that hydrogen can bind to the Zn-ZIF23 leads to positive value of ΔE_{H_2}. On the other hand, hydrogen molecule does not bind with the Zn-ZIF23 host when ΔE_{H_2} is negative value. For the unstable adsorption sites, the hydrogen adsorption energy is set to be zero.

Fig. 5 Hydrogen binding energies of the M-ZIF23 at MN_2 and MN_3 (M = Be, Zn and Cd) adsorption sites.

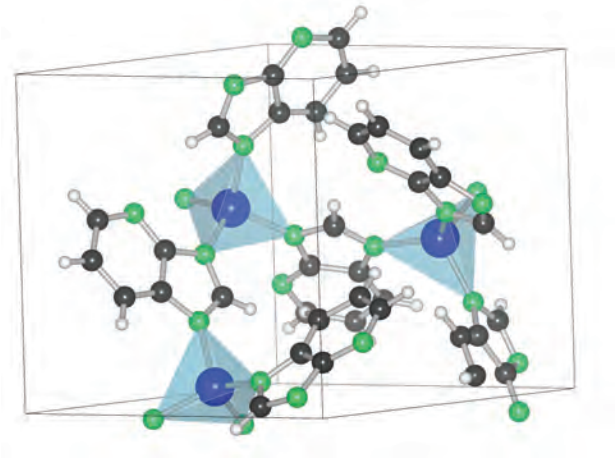

Fig. 1.

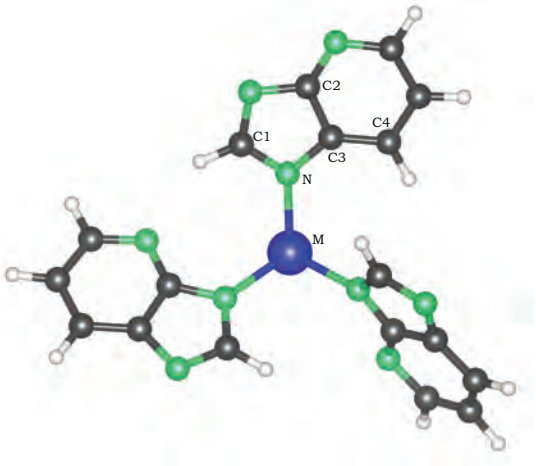

M-ZIF23	M–N (Å)	N–M–N (°)	N–C1 (Å)	C2–C3 (Å)	C3–C4 (Å)
Be-ZIF23	1.79	109.49	1.36	1.42	1.40
Zn-ZIF23	2.05	109.45	1.35	1.42	1.40
Cd-ZIF23	2.25	109.20	1.35	1.42	1.40
Zn-ZIF23 (Exp)[24]	2.01	109.00	1.34	-	1.39

Fig. 2.

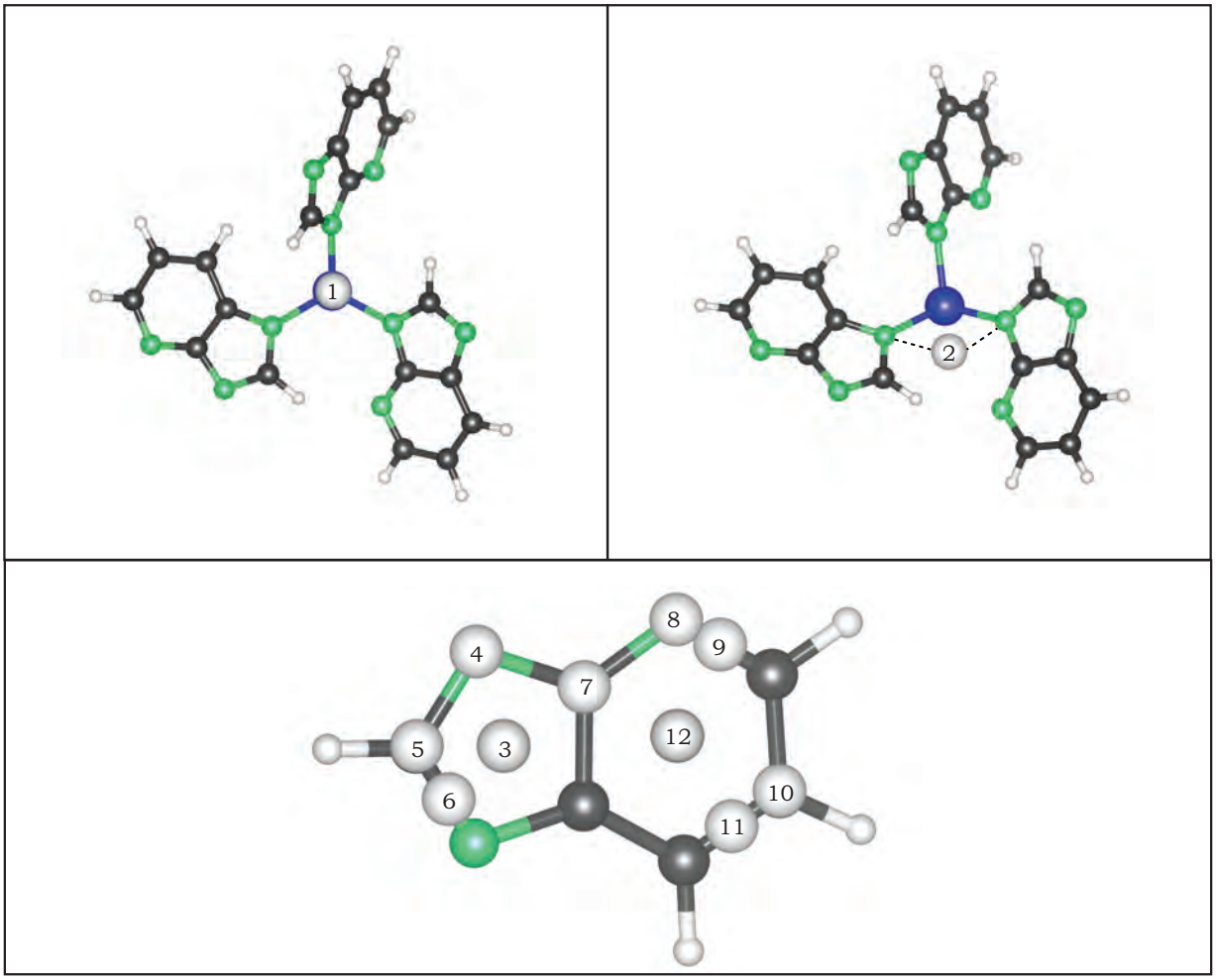

Fig. 3.

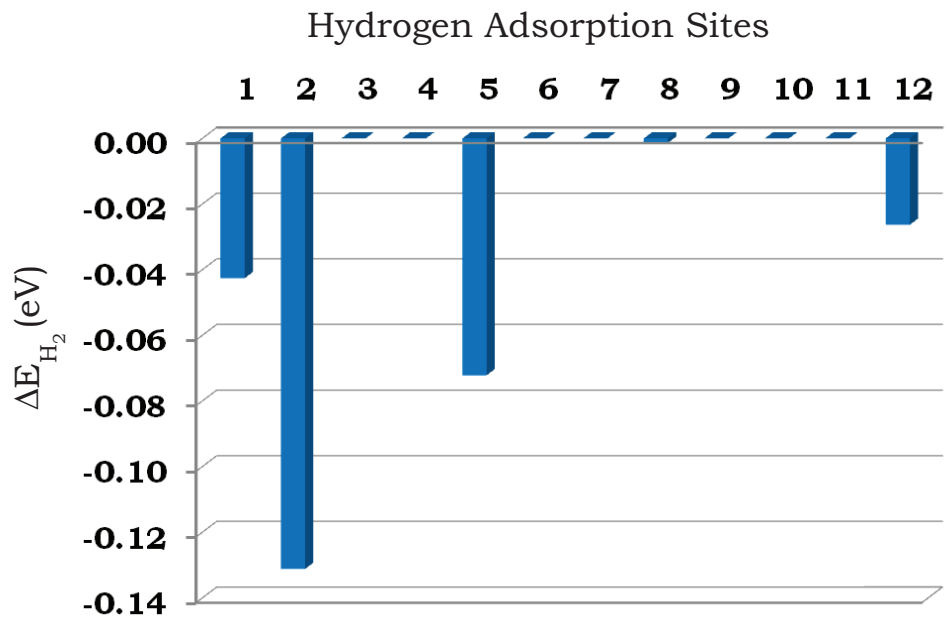
Hydrogen Adsorption Sites
1 2 3 4 5 6 7 8 9 10 11 12
0.00
-0.02
-0.04
-0.06
-0.08
-0.10
-0.12
-0.14
ΔE_{H_2} (eV)

Fig. 4.

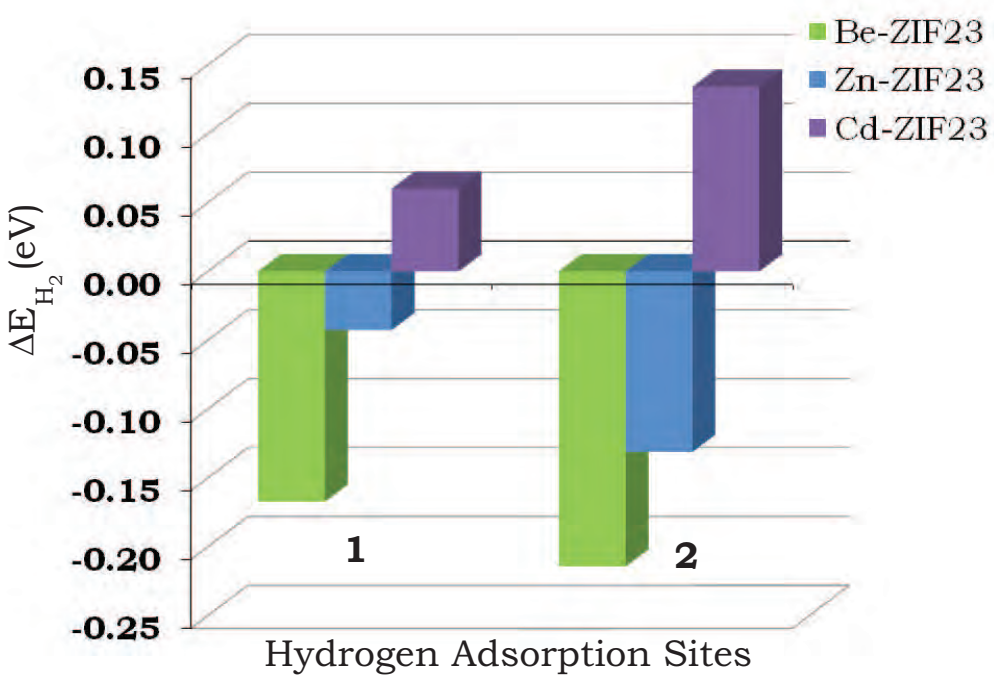
Be-ZIF23
Zn-ZIF23
Cd-ZIF23
0.15
0.10
0.05
0.00
-0.05
-0.10
-0.15
-0.20
-0.25
ΔE_{H_2} (eV)
1
2
Hydrogen Adsorption Sites

Fig. 5.